Long-range Heisenberg models in quasiperiodically driven crystals of trapped ions

A. Bermudez, L. Tagliacozzo, G. Sierra, and P. Richerme

Long-range Heisenberg models in quasi-periodically driven crystals of trapped ions

A. Bermudez,[1,2] L. Tagliacozzo,[3] G. Sierra,[4] and P. Richerme[5]

[1]*Department of Physics, Swansea University, Singleton Park, Swansea SA2 8PP, United Kingdom*
[2]*Instituto de Física Fundamental, IFF-CSIC, Madrid E-28006, Spain*
[3]*Department of Physics and SUPA, University of Strathclyde, Glasgow G4 0NG, United Kingdom*
[4]*Instituto de Física Teórica (IFT), UAM-CSIC, Madrid, Spain*
[5]*Department of Physics, Indiana University, Bloomington, Indiana 47405, USA*

We introduce a theoretical scheme for the analog quantum simulation of long-range XYZ models using current trapped-ion technology. In order to achieve fully-tunable Heisenberg-type interactions, our proposal requires a state-dependent dipole force along a single vibrational axis, together with a combination of standard resonant and detuned carrier drivings. We discuss how this quantum simulator could explore the effect of long-range interactions on the phase diagram by combining an adiabatic protocol with the quasi-periodic drivings, and test the validity of our scheme numerically. At the isotropic Heisenberg point, we show that the long-range Hamiltonian can be mapped onto a non-linear sigma model with a topological term that is responsible for its low-energy properties, and we benchmark our predictions with Matrix-Product-State numerical simulations.

I. INTRODUCTION

The dream of designing the Hamiltonian of an atomic system $H(t)$ to reproduce a relevant model of condensed-matter or high-energy physics H_{target}[1] is already an experimental reality. Quantum-optical setups of neutral atoms[3] and trapped ions[4] have become highly-controllable platforms to address the quantum many-body problem from a different perspective, opening interesting prospects for the short term[2]. Often, the theoretical goal is to describe the dynamics of these systems by a combination of unitaries ($\hbar = 1$)

$$U(t) := \mathcal{T}\left\{ e^{-i\int_0^t d\tau H(\tau)} \right\} \to U_{\text{eff}}(t) := U_0(t) e^{-iH_{\text{eff}}t}, \quad (1)$$

where $U_0(t)$ depends on the scheme used to target the desired model $H_{\text{eff}} = H_{\text{target}}$. This can be accomplished by Trotterizing the time evolution[5], or by using an always-on Hamiltonian, which leads to the notions of digital/analog quantum simulators (QS). For periodic Hamiltonians $H(t) = H(t + T)$, an exact identity can be found $U(t) = U_{\text{eff}}(t)$ by Floquet theory[6]. This has led to the concept of *Floquet engineering* and has important applications in ultracold atoms[7]. To gain further tunability over H_{eff}, one may use a collection of drivings with different periodicities that need not be commensurate. However, a rigorous generalisation of Floquet theory to these *quasi-periodic drivings* is still an open problem[8]. One thus searches for schemes where Eq. (1) is achieved approximately $U(t) \approx U_{\text{eff}}(t)$, but with sufficient accuracy, and where the additional effects brought up by $U_0(t)$ are not in conflict with the target model of the analog quantum simulator.

In trapped ions[9], an analog QS (1) for the quantum Ising model, a paradigm of phase transitions[13,14], has already been achieved[10–12]. Unfortunately, implementing what is arguably the most important model of low-dimensional magnetism[15–17], the so-called *XYZ model*[20]

$$H_{\text{XYZ}} = \sum_{i>j} \left(J_{ij}^x \sigma_i^x \sigma_j^x + J_{ij}^y \sigma_i^y \sigma_j^y + J_{ij}^z \sigma_i^z \sigma_j^z \right), \quad (2)$$

where J_{ij}^α and σ_i^α are coupling strengths and Pauli matrices for $\alpha \in \{x, y, z\}$, has remained elusive for several years. Although

the digital QS of this model has already been achieved[18], and a combination of digital and analog protocols proposed[19], it would be desirable to find purely-analog QS that can be scaled to larger ion crystals without the need of quantum error correction to mitigate Trotterization errors.

In this work, we present such a scheme using quasi-periodic drivings. To implement a rotated XXZ model $H_{\text{eff}} = H_{\text{XXZ}}$ obtained from (2) after setting $J_{ij}^y = J_{ij}^z$,[21] our scheme only requires modifying the driving fields that produce an effective Ising model[11]. Moreover, we show that the XYZ model can be achieved $H_{\text{eff}} = H_{\text{XYZ}}$ by introducing additional drivings. We test the validity of our proposal against numerical simulations, and present a detailed study of the effect of the long-range interactions that arise naturally in ion traps, and break the integrability of the model[17,20,21].

This article is organized as follows. In Sec. II, we describe the scheme based on quasi-periodic drivings that leads to an effective XYZ model for a trapped-ion crystal. We analyze the suitability of this scheme with respect to experimentally-available tools in Sec. III, and test its validity by comparing the analytical predictions to numerical simulations in Sec. IV. In Sec. V, we derive an effective quantum field theory to describe the low-energy properties of the effective long-range XYZ model in the SU(2) symmetric regime, and tests some of its predictions using numerical algorithms based on Matrix-Product-States. Finally, we present our conclusions in Sec. VI. Details of the different derivations in these sections are given in the Appendixes.

II. QUASI-PERIODICALLY DRIVEN IONS

We consider a trapped-ion chain subjected to different drivings between two electronic states $|\uparrow\rangle, |\downarrow\rangle$[9]. The bare dynamics is described by $H_0 = \sum_i \frac{\omega_0}{2} \sigma_i^z + \sum_{n,\alpha} \omega_{n,\alpha} a_{n,\alpha}^\dagger a_{n,\alpha}$, where ω_0 is the transition frequency, and $a_{n,\alpha}^\dagger, a_{n,\alpha}$ the phonon creation-annihilation operators in a normal mode of frequency $\omega_{n,\alpha}$[22]. A useful quasi-periodic driving is a dipole force

transversal to the chain, e.g. Mølmer-Sørensen (MS)[23] force

$$H_{\text{MS}} = \sum_{i,n} \mathcal{F}_{in} x_0 \sigma_i^+ \left(a_{n,x} e^{i\phi_r - i\omega_r t} + a_{n,x}^\dagger e^{i\phi_b - i\omega_b t} \right) + \text{H.c.}, \quad (3)$$

where we have introduced the light forces $\mathcal{F}_{in}$, the zero-point motion x_0 along the x axis, $\sigma_i^+ = |\uparrow_i\rangle\langle\downarrow_i|$, and the frequencies $\omega_r = \omega_0 - \omega_{n,x} + \delta_n, \omega_b = \omega_0 + \omega_{n,x} - \delta_n$, and phases ϕ_r, ϕ_b, of two laser beams (see below). Another useful periodic driving follows from a laser/microwave coupled to the transition

$$H_{\text{C},1} = \sum_i h_0 \sigma_i^+ e^{i\phi_d - i\omega_d t} + \text{H.c.}, \quad (4)$$

where h_0 is half the Rabi frequency, and we have introduced the driving frequency ω_d, and phase ϕ_d.

As shown in theory and experiments[10,11], the quasi-periodic Hamiltonian $H(t) = H_0 + H_{\text{MS}} + H_{\text{C},1}$, in the regime

$$h_0 \ll \mathcal{F}_{in} x_0 \ll \delta_n \ll \omega_{n,x}, \quad \omega_d = \omega_0, \quad (5)$$

leads to a time-evolution of the form (1) with $U(t) \approx U_{\text{eff}}(t)$ targeting a long-range quantum Ising model $H_{\text{eff}} = H_{\text{QIM}}$

$$H_{\text{QIM}} = \sum_{i>j} J_{ij} \sigma_i^{\phi_s} \sigma_j^{\phi_s} + h_0 \sum_i \sigma_i^{\phi_d}. \quad (6)$$

Here, we have introduced the spin-spin couplings $J_{ij} = -\sum_n \mathcal{F}_{in} \mathcal{F}_{jn}^* x_0^2/\delta_n + \text{c.c.}$, $\sigma_i^\theta = \sigma_i^+ e^{i\theta} + \text{H.c.}$, and the spin phase $\phi_s = (\phi_r + \phi_b)/2 + \pi/2$ of the MS lasers. Provided that the phases fulfil $\phi_s = \phi_d + \pi/2$, the engineered Hamiltonian (6) corresponds to a transverse-field Ising model[13,14]. We note that the additional unitary in (1) is simply $U_0(t) = e^{-itH_0}$, which does not compromise the measurement in the QS, e.g. magnetisation and spin correlations.

As outlined in[10], by combining three dipole forces along each vibrational axis, one may exploit all phonon branches to mediate a Heisenberg-type interaction (2). However, in addition to the technical overhead of combining all the required laser beams, there are some fundamental limitations. Since the axial trap frequency must decrease with the number of ions, the spin-spin interactions mediated by axial phonons become weaker as the crystal grows. This becomes especially troublesome as the $J_{ij}^z \sigma_i^z \sigma_j^z$ interactions require a differential ac-Stark shift, and thus exclude using clock states[24], making the experiment less resilient to magnetic-field fluctuations. Moreover, the distance dependence of axial- and transverse-mediated interactions differs markedly[10], such that the important SU(2)-symmetric point $J_{ij}^x = J_{ij}^y = J_{ij}^z$ cannot be achieved. Although some of these problems may be circumvented with surface traps[25], it would be desirable to implement Heisenberg-type models with current Paul/Penning designs[11,26], which requires using a single branch of transverse phonons to mediate the interactions. Our main result is to present such scheme by combining the MS force (3), such that clock states can be used to encode the spin, with a carrier term (4) supplemented by two additional tones

$$H_{\text{C},3} = \sum_i \sum_{t=1,2,3} h_t \sigma_i^+ e^{i\phi_{d,t} - i\omega_{d,t} t} + \text{H.c.}, \quad (7)$$

Table I. **Parameters of the three-tone driving in Eq.** (7)

Tone	$t=1$	$t=2$	$t=3$
Frequency	$\omega_{d,1} = \omega_0$	$\omega_{d,2} = \omega_0 + \Delta$	$\omega_{d,3} = \omega_0 - \Delta$
Strength	$h_1 = h_0$	$h_2 = \frac{1}{2}h_0\xi$	$h_3 = \frac{1}{2}h_0\xi$
Phase	$\phi_{d,1} = 0$	$\phi_{d,2} = 0$	$\phi_{d,3} = 0$

symmetrically detuned with respect to the carrier transition (see Table I). We show that the quasi-periodically driven Hamiltonian $H(t) = H_0 + H_{\text{MS}} + H_{\text{C},3}$, leads to $U(t) \approx U_{\text{eff}}(t)$ described by the XYZ model $H_{\text{eff}} = H_{\text{XYZ}}$ (2), where the spin-spin interactions

$$J_{ij}^x = J_{ij} \cos^2 \phi_s, \quad J_{ij}^{y/z} = \frac{1}{2} J_{ij} \sin^2 \phi_s (1 \mp \mathcal{J}_1(\xi)), \quad (8)$$

are expressed in terms of the J_{ij} couplings introduced below Eq. (6), and the first-order Bessel function $\mathcal{J}_1(x)$. Varying the spin phase ϕ_s allows for independent control over J_{ij}^x and $J_{ij}^{y/z}$, while varying the drive strengths h_2 and h_3 controls the asymmetry between J_{ij}^y and J_{ij}^z. Moreover, the additional unitary in (1) is $U_0(t) = e^{-itH_0} e^{-i\sum_i h_0(t + \xi \sin(\Delta t)/\Delta)\sigma_i^x}$.

We now address the crucial task of finding the parameter regime that substitutes Eq. (5), and gives rise to a XYZ model (2) instead of the usual Ising model (6). Previous results found that by modifying the strength of the driving (4), one either obtains a new Ising model with the phase of the driving for $\mathcal{F}_{in}x_0 \ll \delta_n \ll h_0$[27], or an isotropic XY model for milder drivings $\max\{\mathcal{F}_{in}x_0, h_0\} \ll \delta_n$, and $J_{ij} \ll h_0$[28]. If instead of the resonant driving (4), a periodically-modulated one is considered, it is possible to engineer an anisotropic XY model[29]. We also note that more generic periodic drivings with a site-dependent phase allow to control also the directionality of the XY interactions, and achieve effective spin Hamiltonians corresponding to quantum compass models[30].

These results thus suggest that we should combine resonant and off-resonant drivings, as in Eq. (7), and explore the regime of large, but not too strong, driving strengths.

By using the Magnus expansion[31], together with techniques for periodically-modulated systems[7,32] (see Appendix A), we find that the regime to obtain a XYZ model (2) is

$$\max\{\mathcal{F}_{in}x_0, h_0, \Delta\} \ll \delta_n \ll \omega_{n,x}, \quad \xi < \frac{1}{2}, \quad (9)$$

together with

$$\max\{J_{ij}\} \ll 2h_0, \quad \Delta = 4h_0. \quad (10)$$

Condition (9) is important to *(i)* avoid that the drivings perturb the laser-ion interaction leading to the MS force (3), and *(ii)* minimise residual spin-phonon terms impeding a description of the spin dynamics by a periodically-modulated Ising model

$$H_{\text{eff}}(t) = \sum_{i>j} J_{ij} \sigma_i^{\phi_s}(t) \sigma_j^{\phi_s}(t), \quad \sigma_i^{\phi_s}(t) = \hat{U}(t) \sigma_i^{\phi_s} \hat{U}(t)^\dagger, \quad (11)$$

where $\hat{U}(t) = e^{-i\sum_i h_0(t + \xi \sin(\Delta t)/\Delta)\sigma_i^x}$. Finally, condition (10) guarantees that *(iii)* this periodically-modulated Ising model leads to the desired XYZ Hamiltonian (2).
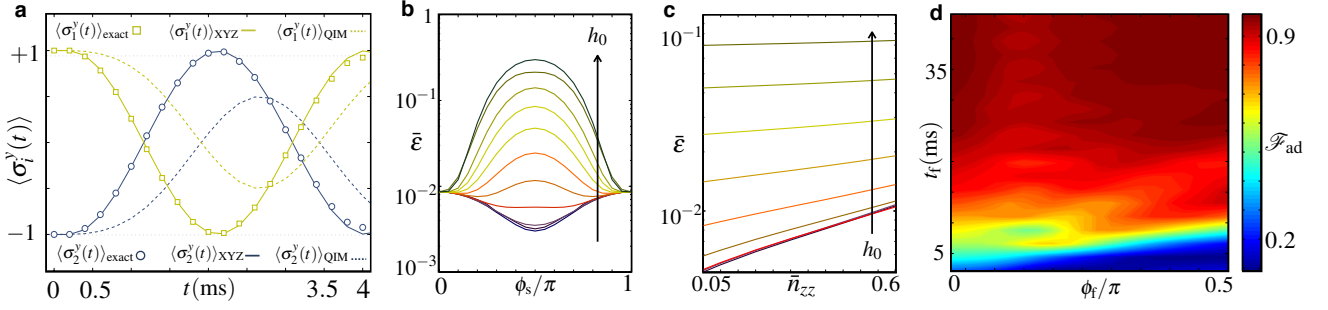
Figure 1. **Numerical validation of the XYZ Heisenberg model:** **(a)** Magnetization dynamics $\langle\sigma_i^y(t)\rangle_\beta$ for a two-ion chain evolving under $\beta \in \{\text{exact}, \text{XYZ}\ (2), \text{QIM}\ (6)\}$. The trapped-ion parameters for the MS (3) are $\delta/2\pi = 500$kHz, $\Omega_L/2\pi = 0.9$MHz, and $\phi_s = \pi/3$; whereas for the modulated carrier (7) in Table I, $h_0/2\pi = 2.5$kHz, $\xi = 0.09$ and $\Delta/2\pi = 10$kHz. We consider initial mean phonon numbers $\bar{n}_{zz} = 0.05$, and $\bar{n}_{com} = 0.047$, and truncate the vibrational Hilbert space to 7 phonons per mode. To ease the visualisation, we perform a spin-echo refocusing pulse at the middle $U_s = e^{i\frac{\pi}{2}\sum\sigma_i^y}$ for different evolution times given by multiples of $\pi/h_0 = 4\pi/\Delta$. **(b,c)** Quantum channel error as a function of **(b)** the MS phase ϕ_s, and **(c)** the mean number of phonons in the lowest mode, considering for the same parameters, but setting $\Omega/2\pi = 0.5$MHz, and varying $h_0/2\pi \in \{1.2, 1.8, 2.4, 3, 3.6, 4.2, 4.8, 5.3, 5.9\}$kHz, and the associated detunings $\Delta = 4h_0$. The different lines correspond to the above values of h_0 increasing in the direction of the arrow. **(d)** Adiabatic evolution of $|\psi_0\rangle = |-_y +_y -_y +_y -_y +_y\rangle$ for $N = 6$ ions, subjected to *(i)* an Ising linear ramp $t \in [0, t_f/2]$ of the staggered field $h_0(t) = h_0(0) - \delta h t$, with $h_0(0) = 12J_{12}$, and $\delta h = -2h_0(0)/t_f$, followed by *(ii)* a Heisenberg linear ramp $t \in [t_f/2, t_f]$ of the phase $\phi_s(t) = \delta\phi t$, where $\delta\phi = 2\phi_f/t_f$, as described in the text. The adiabatic fidelity $\mathscr{F}_{ad}$ is represented as a function of the total ramp time t_f, which is set to be an integer multiple of $2\pi/h_0$, and the final phase ϕ_f.

III. EXPERIMENTAL CONSIDERATIONS FOR THE SCHEME

While our results are applicable to most ion species, and to Penning traps, we focus on a chain of ^{171}Yb$^+$ ions in a linear Paul trap biased to yield transverse and axial trap frequencies of 5 MHz and 1 MHz, respectively, and 2-3 μm ion spacing[28]. Within each Yb ion, the $^2S_{1/2}|F = 0, m_F = 0\rangle$ and $^2S_{1/2}|F = 1, m_F = 0\rangle$ hyperfine 'clock' states, denoted $|\uparrow\rangle$ and $|\downarrow\rangle$ respectively, encode the effective spin-1/2 system[33].

The spin-spin interaction and external magnetic field in Eq. (6) are routinely generated by globally driving stimulated Raman transitions between the spin states[11]. Two Raman beams are aligned with their wavevector difference along the transverse vibrational axis $\mathbf{e}_x$ (see Appendix A). One is held at fixed frequency ω_L, while the other contains multiple frequencies $\omega_L + \delta\omega_\ell$ imprinted by an acousto-optic modulator (AOM). The AOM is driven by an arbitrary waveform generator (AWG), allowing for full frequency, amplitude, and phase control over the components of the second Raman beam. For instance, simultaneous application of $\delta\omega_\ell \in \{\omega_r, \omega_b\}$ with respective phases $\{\phi_r, \phi_b\}$ will lead to a MS force (3) that yields the first term of (6) if the parameters fulfil (5). Additionally, applying $\delta\omega_\ell = \omega_0$ with phase ϕ_d leads to (4) and yields the second term of Eq. (6). Typical parameters are a carrier Rabi frequency $\Omega_L/2\pi \sim 0.1\text{-}1$ MHz, a Lamb-Dicke parameter $\eta = 0.07$, and a MS detuning $\delta_n/2\pi \sim 100\text{-}500$ kHz, giving a maximum spin-spin coupling $J_{max}/2\pi \sim 0.1\text{-}1$ kHz. In the current scheme, choosing $h_0/2\pi \sim 1\text{-}10$ kHz simultaneously satisfies the conditions in Eqs. (9) and (10), and is easily achievable given the large carrier Rabi frequency. We also note that the typical mean number of phonons after laser cooling in the resolved-sideband regime is $\bar{n}_n \sim 0.05\text{-}0.1$.

Realizing a XYZ interaction according to our scheme in-

volves two additional tones (7), requiring a simple reprogramming of the AWG to provide the simultaneous frequencies $\delta\omega_\ell \in \{\omega_r, \omega_b, \omega_0, \omega_0 + \Delta, \omega_0 - \Delta\}$ along with the respective phases $\{\phi_r, \phi_b, 0, 0, 0\}$. Alternatively, the AWG can be programmed to modulate the amplitude of the ω_0 tone as $h_0(1 + \xi\cos(\Delta t))$; such modulations have already been a key technique in trapped-ion many-body spectroscopy[43]. While possible experimental limitations could include the sampling rate of the AWG (> 1 GHz) and the response rate of the AOM (>20 MHz), these are both sufficiently fast to allow for the desired modulations ($\Delta/2\pi \approx 20$ kHz).

IV. NUMERICAL VALIDATION OF THE SCHEME

sec:num We start by visualising $\langle\sigma_i^y(t)\rangle$ for a two-ion setup with the parameters in Fig. 1. The spin-phonon system is initialised in $\rho(0) = |\psi_0\rangle\langle\psi_0| \otimes \rho_{th}$, where $|\psi_0\rangle = |+_y\rangle|-_y\rangle$ is the spin state, $|\pm_y\rangle$ are the eigenstates of σ^y, and ρ_{th} is the vibrational thermal state after laser cooling. In Fig. 1**(a)**, we compare the prediction of the full Hamiltonian $H(t)$ with the XYZ (2) and the $h_0 = 0$ Ising model (6), which clearly shows that the magnetisation exchange is no longer described by the Ising model, but instead by the XYZ model. To quantify the accuracy, we determine how close the exact and effective evolutions are, regardless of the possible initial states and observables, via the quantum channel fidelity $\mathfrak{F}(t) := \int d\psi_s \langle\psi_s| U_{eff}^\dagger(t)\mathscr{E}(|\psi_s\rangle\langle\psi_s|)U_{eff}(t)|\psi_s\rangle$, where $\mathscr{E}(|\psi_s\rangle\langle\psi_s|) := \text{tr}_{ph}\{U(t)|\psi_s\rangle\langle\psi_s| \otimes \rho_{th}U^\dagger(t)\}$, and one integrates over the Haar measure $d\psi_s$. This quantity can be evaluated efficiently[34], although the numerics become considerably more demanding. Hence, we focus on the XXZ model (8) for $\xi = 0$[35], and believe that the results should be similar for the XYZ case. In Fig. 1, we represent the time-averaged error $\bar{\varepsilon} = \frac{1}{t_f}\int_0^{t_f} dt(1 - \mathfrak{F}(t))$, where $t_f = \pi/J_{12}$, as a function of: **(b)**

the spin phase ϕ_s that controls the XXZ parameters (8), and **(c)** the mean phonon number. These results show that the accuracy of the XXZ model in representing the full spin-phonon dynamics is above 99% if $h_0/2\pi <$2kHz, for all phases ϕ_s, and for warm phonons up to $\bar{n}_n < 0.5$. In particular, they show that phonon-induced errors are negligible in the parameter regime (9), which will allow us to study adiabatic protocols to prepare the XXZ model groundstate by looking directly at the periodically-modulated spin model (11).

The nearest-neighbour limit of the XXZ model hosts two different phases: a gapped antiferromagnetic phase for $\phi_s < \phi_s^c := \cos^{-1}(1/\sqrt{3})$, and a gapless Luttinger liquid for $\phi_s > \phi_s^{c\,36}$. The addition of frustration via next-to-nearest-neighbour interactions leads to a richer phase diagram with additional spontaneously dimerised[37] and gapless chiral[38] phases. The fate of these phases in presence of long-range interactions (2) is an open question, which could be addressed with our setup if *(i)* preparation and *(ii)* detection of the groundstate are shown to be possible. We start by discussing initialisation via adiabatic evolution and the role of the Hamiltonian symmetries for finite chains. For $N/2$ even, we choose $|\psi_0\rangle = |-_y -_y -_y \cdots\rangle$, which can be prepared using global one-qubit gates, and approximates the paramagnetic groundstate of the Ising model (6) for $\phi_s = 0$, $\phi_d = \pi/2$, and $h_0 \gg J_{ij}$. For $N/2$ odd, we choose $|\psi_0\rangle = |-_y +_y -_y \cdots\rangle$, which approximates the groundstate of a staggered Ising model[39]. One then ramps down $h_0(t) \to 0$ slowly, such that the state adiabatically follows the groundstate of the Hamiltonian and ends in one of the Ising groundstates $|\psi_p\rangle = \frac{1}{\sqrt{2}}\left(1 + p \otimes_{i=1}^{N} \sigma_i^z\right)|+_x -_x +_x \cdots\rangle$, where the parity $p = +1$ for $N/2$ even, and $p = -1$ for $N/2$ odd, is related to the $\mathbb{Z}_2$ symmetry of the Hamiltonian. This even-odd distinction is crucial for the rest of the protocol, where the additional tones (7) in Table I are switched on, making sure that the constraints (9)-(10) are fulfilled, and the spin phase is slowly ramped up to the desired value $\phi_s(t) \to \phi_f$. We expect to have prepared the groundstate of the long-range XXZ model (2) corresponding to that particular ϕ_f, which has parity $p = \pm 1$ for $N/2$ even/odd as a consequence of the open boundary conditions of the finite chain[40]. In Fig. 1**(d)**, we represent the fidelity $\mathscr{F}_{\rm ad}(t_f, \phi_f) = |\langle \varepsilon_{\rm gs}^{\rm XXZ}(\phi_f)|\psi(t_f)\rangle|^2$, where $|\psi(t_f)\rangle = \mathscr{T}\{e^{-i\int_0^{t_f} d\tau H(\tau)}\}|\psi_0\rangle$ is the state evolving under the succession of the Ising (6) and the periodically-modulated (11) spin Hamiltonians, according to the previous sequence of adiabatic ramps, and $|\varepsilon_{\rm gs}^{\rm XXZ}(\phi_f)\rangle$ is the exact groundstate of (2). We observe that the fidelity is very close to unity when the ramps are slow enough. For fast ramps, the fidelities are compromised in the region $\phi_f > \phi_s^c \approx 0.3\pi$, which is a consequence of a decrease in the energy gap, and would become accentuated as N grows[42].

Once the desired ground states are adiabatically prepared, we can address the issue of detection. Trapped-ion experiments allow in-situ measurements of spin-spin correlations through fluorescence[11], or spectroscopic probes of low-lying excitations[43]. The former would allow to distinguish between Ising, Luttinger, dimerised, and spin-chiral orders discussed above, whereas the later would probe their gap.

V. LONG-RANGE HEISENBERG MODEL

To get a flavour of the effect of long-range interactions in our quantum simulator (2), we focus on the archetypical SU(2)-symmetric point $\phi_s = \phi_s^c$, $\xi = 0$. In analogy to Haldane's result for the nearest-neighbour model[44], we map the low-energy properties of our long-range Heisenberg Hamiltonian onto a non-linear sigma model (NLSM) described by the Lagrangian

$$\mathscr{L}_{\rm NLSM} = \frac{1}{2g}(\partial_\mu \boldsymbol{\phi}) \cdot (\partial^\mu \boldsymbol{\phi}) + \frac{\Theta}{8\pi}\varepsilon^{\mu\nu}\boldsymbol{\phi} \cdot (\partial_\mu \boldsymbol{\phi} \times \partial_\nu \boldsymbol{\phi}). \quad (12)$$

Here, $\boldsymbol{\phi}(x^\mu)$ is a three-component vector field associated to the staggered magnetisation, constrained to $|\boldsymbol{\phi}|^2 = 1$, and defined on a 1+1 space-time $x^\mu = (vt, x)$. We have introduced the velocity $v = a_0(\sum_r \tilde{J}_{2r-1}\chi)^{1/2}$, where a_0 is the lattice spacing for bulk ions, $\tilde{J}_r = 4J_{i,i+r}$, and $\chi = \sum_r(-1)^{r+1}r^2\tilde{J}_r$. Additionally, we get a coupling constant $g = 2(\sum_r \tilde{J}_{2r-1}\chi^{-1})^{1/2}/S$, and a topological angle $\Theta = \pi$ (see Appendix B).

The topological Θ-term has drastic consequences on the NLSM. Under a renormalisation-group transformation, it either flows to the gapless fixed point of the SU(2)$_1$ Wess-Zumino-Witten (WZW) conformal field theory when $g < g_c$, or to a gapped fixed point for $g > g_c$[45]. Truncating the long-range to two neighbours, one finds $g = 4/\sqrt{1 - 4\tilde{J}_2/\tilde{J}_1}$, such that $g \to \infty$ as $\tilde{J}_2 \to \tilde{J}_1/4$. This coincides roughly with the critical point towards the spontaneously dimerised phase of the J_1-J_2 Heisenberg model[37], which is a truncation of the lattice version of the SU(2)$_1$ WZW theory: the Haldane-Shastry model[46,47]. Therefore, the NLSM mapping identifies the WZW critical point with the instability $g_c \to \infty$.

For the full long-range model (2), the distance-decay of the spin-spin interactions in the trapped-ion crystal is

$$\tilde{J}_r \approx 4\frac{|J_0\lambda|}{|r|^3} + 8|J_0|\big(\mathrm{sgn}(\lambda)\big)^{1+r}\mathrm{e}^{-\frac{|r|a_0}{\xi_0}}\theta(r-2), \quad (13)$$

where J_0 quantifies the spin couplings, λ determines how close the MS forces lie from the vibrational sidebands, and $\xi_0 \approx -a_0/\log(|\lambda|)$ for far-detuned forces $|\lambda| \ll 1$(see Appendix C). We find that $g \approx \sqrt{7\zeta(3)/2 + 2\lambda}/\sqrt{\log 2 - 2\lambda}$, where $\zeta(n)$ is the Riemann zeta function. For $|\lambda| \ll 1$, the NLSM coupling is thus finite, and no instability takes place. Therefore, the NLSM predicts that our long-range Heisenberg model flows to the WZW fixed point (i.e. gapless, power-law correlations, and logarithmic scaling of the entanglement entropy), instead of the spontaneously dimerised gapped phase.

We test this prediction numerically by a Matrix-Product-state calculation of the ground-state entanglement entropy $S_\ell = -\mathrm{Tr}\{\rho_\ell \log\rho_\ell\}$, where $\rho_\ell = \mathrm{Tr}_{N-\ell}\{|\varepsilon_g\rangle\langle\varepsilon_g|\}$ is the reduced density matrix for a block of ℓ sites inside a chain of length N. In Fig. 2, S_ℓ is depicted for different block sizes as a function of $y_\ell = \log(\frac{2N}{\pi}\sin(\frac{\pi\ell}{N}))$, and considering different interaction ranges (13). For a chain with open boundary conditions, conformal field theory predicts $S_\ell = \frac{c}{6}y_\ell + a$, where c is the central charge, and a is a non-universal constant[54]. Our numerical results display the predicted linear scaling of a gapless phase but, interestingly, long range interactions change
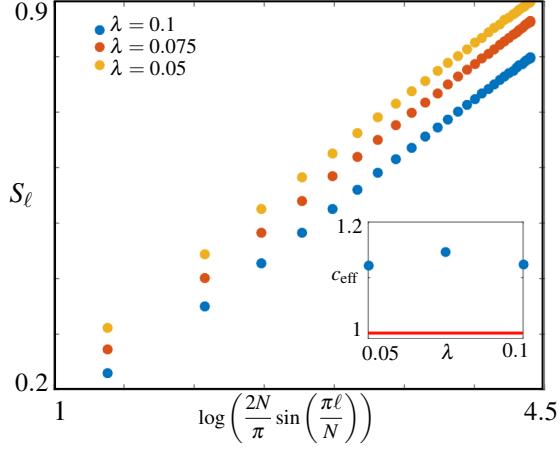
Figure 2. **Central charge in the long-range Heisenberg model:** Entanglement entropies S_ℓ of blocks of length ℓ in a chain of $N = 128$ spins computed with a Matrix-Product-State ansatz for the ground state of the long range Heisenberg model with couplings (13) using bond dimensions up to 200 to guarantee the convergence of the ground state energy up to 12 digits. The ground state is obtained using the time-dependant variational algorithm originally presented in[51] and later reformulated for finite chains with long range interactions in[52,53]. The entanglement entropies, for large enough ℓ scale linearly with the variable $y_\ell = \log(\frac{2N}{\pi}\sin(\frac{\pi\ell}{N}))$, as expected for a conformally-invariant spin chain, for all the values considered $\lambda \in \{0.1, 0.075, 0.05\}$. Quantitatively, the pre-factor of the scaling exceeds the central charge $c = 1$ of the nearest-neighbor model (red line). The coefficients c_{eff} are obtained by a linear fit of the larger ℓ entropies to $S_\ell = \frac{c_{eff}}{6} y_\ell + a$, and shown in the inset.

quantitatively the value of the central charge, which gets promoted from the short-range prediction $c = 1$ to an effective larger value $c_{eff} > 1$[55] (see inset in Fig. 2). A similar behavior had already been observed in the long-range quantum Ising model at criticality[52], and we provide a possible qualitative explanation of both below.

This effect can be understood qualitatively from the scaling of S_ℓ in closed spin chains with a defect[54,56], namely a weaker spin-spin coupling $0 \leq J_d \leq J$ in a particular bond. Depending on the particular model, one can find $S_\ell = \frac{c_{eff}}{6} y_\ell + a'$ with c_{eff} varying continuously with J_d between the open- and closed-chain limits $c \leq c_{eff} \leq 2c$. Our numerics show a similar behavior, which can be understood intuitively by noticing that long-range interactions induce direct couplings between the otherwise non-interacting boundaries of the chain, yielding a hybrid between the closed- and open-chain limits. Accordingly, one would expect $c_{eff} > c$, which is the result found in the inset of Fig. 2.

VI. CONCLUSIONS AND OUTLOOK

We have proposed a realistic QS of long-range Heisenberg-type models based on quasi-periodically driven trapped ions. Making use of a single branch of phonons, this scheme is readily applicable to existing experiments that simulate the Ising model in either Paul[11] or Penning[26] traps. Since the Heisenberg model describes the magnetic properties of Mott-insulating materials, our work opens the possibility of using trapped-ion quantum simulators to assess real-world problems. We have presented analytic and numerical evidence that the 1D long-range model shares similar topological properties with the paradigmatic nearest-neighbour limit[44]. It would be very interesting to generalise these methods to ladders with triangular motifs, as these arise naturally in the experiment, and may provide an alternative to observe non-trivial effects[48] that appear in integer-spin Heisenberg models[44,49,50].

Appendix A: Derivation of the effective long-range XYZ model

In this Appendix, we present a detailed derivation of the effective Heisenberg-type XYZ model (2) directly from the Hamiltonian of the periodically-driven trapped-ion chain $H(t) = H_0 + H_{MS} + H_{C,3}$ in Eqs. (3), and (7). For the shake of completeness, however, we note that: *(i)* the un-driven trapped-ion crystal is described by H_0 in the harmonic approximation, which is valid for low-enough temperatures and small vibrations around the equilibrium positions[22]. *(ii)* The Mølmer-Sørensen force H_{MS} (3) is obtained from the light-matter interaction of a pair of laser beams[23] coupled to the internal transition in the regime of resolved sidebands[9], such that the frequency of one laser is tuned to the first red sideband $\omega_r = \omega_0 - \omega_{n,x} + \delta_n$, whereas the other laser excites the first blue sideband $\omega_b = \omega_0 + \omega_{n,x} - \delta_n$. These excitations are in practice generated by passing a laser beam through an acousto-optic modulator driven by an arbitrary waveform generator (see Fig. 3(**a**)). When the opposite detunings fulfil $\delta_n \ll \omega_{n,x}$, the light matter interaction yields Eq. (3), where the light forces and zero-point displacement can be expressed as

$$\mathscr{F}_{in} = i\frac{\Omega_L \Delta\mathbf{k} \cdot \mathbf{e}_x}{2}\sqrt{\frac{\omega_x}{\omega_{n,x}}}\mathscr{M}_{i,n}e^{-\frac{1}{2}\sum_n \mathscr{M}_{in}^2 \eta_n^2}, \quad x_0 = \frac{1}{\sqrt{2m\omega_x}} \tag{A1}$$

in terms of the common Rabi frequency (Lamb-Dicke parameter) $\Omega_L \ll \omega_{n,x} \ll \omega_0$ ($\eta_n = \Delta\mathbf{k} \cdot \mathbf{e}_x/\sqrt{2m\omega_{n,x}} \ll 1$) of both MS laser beams, the trap ω_x and normal-mode $\omega_{n,x}$ frequencies, and the corresponding normal-mode displacements $\mathscr{M}_{i,n}$. In Eq. (3), we have written explicitly the phases of the red- and blue-sideband beams ϕ_r, ϕ_b (see Fig. 3(**a**)). *(iii)* The carrier driving $H_{C,3}$ (7) can be obtained from the light-matter interaction with an additional laser beam that pases through the acousto-optic modulator producing three tones with frequencies $\omega_{d,1} = \omega_0$, $\omega_{d,2} = \omega_0 + \Delta$, $\omega_{d,3} = \omega_0 - \Delta$, such that

$\Delta \ll \omega_{n,x}$, which can be also included in the waveform generator. In this later case, the strengths of the carrier drivings are limited to $h_{\rm t} = \Omega_{\rm d,t}/2 \ll \omega_{n,x}/\eta_n$[9]. By virtue of the arbitrary wave generator, it is possible to control not only the driving strengths, but also the phases of the drivings $\phi_{\rm d,t}$ with respect to $\phi_{\rm r}$, and $\phi_{\rm b}$, which allows us to consider the values listed in Table I.

Let us now start with the derivation of the effective XYZ model. The first step is to move to the interaction picture with respect to H_0, $|\tilde{\psi}\rangle = {\rm e}^{{\rm i}H_0 t}|\psi\rangle$, such that ${\rm i}\partial_t |\tilde{\psi}\rangle = (\tilde{H}_{\rm MS}(t) + \tilde{H}_{\rm C,3}(t))|\tilde{\psi}\rangle$, with the following drivings

$$\tilde{H}_{\rm MS}(t) = \sum_{i,n} \mathscr{F}_{in} x_0 \sigma_i^{\phi_{\rm s}} (a_{n,x} {\rm e}^{{\rm i}\phi_{\rm m} - {\rm i}\delta_n t} + a_{n,x}^\dagger {\rm e}^{-{\rm i}\phi_{\rm m} + {\rm i}\delta_n t}), \quad (A2)$$

where in addition to the average spin phase $\phi_{\rm s}$, and the spin operator $\sigma_i^{\phi_{\rm s}}$ introduced below Eq. (6) in the main text, also the relative motional phase $\phi_{\rm m} := (\phi_{\rm r} - \phi_{\rm b})/2$ appears. In this interaction picture, the carrier driving becomes

$$\tilde{H}_{\rm C,3}(t) = \sum_i h_0 \big(1 + \xi \cos(\Delta t)\big)\sigma_i^x, \quad (A3)$$

where we have used the parameters listed in Table I, such that ξ depends on the ratio of the Rabi frequencies of the $\pm\Delta$ detuned tones with respect to the resonant one. Let us now perform the following unitary transformation $|\hat{\psi}\rangle = \hat{U}(t)|\tilde{\psi}\rangle$, with

$$\hat{U}(t) = {\rm e}^{{\rm i}\sum_i h_0 \left(t + \frac{\xi}{\Delta}\sin(\Delta t)\right)\sigma_i^x}, \quad (A4)$$

such that the transformed state evolves only under the transformed MS force ${\rm i}\partial_t |\hat{\psi}\rangle = \hat{H}_{\rm MS}(t)|\hat{\psi}\rangle$, namely

$$\hat{H}_{\rm MS}(t) = \sum_{i,n} \mathscr{F}_{in} x_0 \sigma_i^{\phi_{\rm s}}(t)(a_{n,x}{\rm e}^{{\rm i}\phi_{\rm m} - {\rm i}\delta_n t} + a_{n,x}^\dagger {\rm e}^{-{\rm i}\phi_{\rm m} + {\rm i}\delta_n t}). \quad (A5)$$

Here, we have introduced the transformed spin operator $\sigma_i^{\phi_{\rm s}}(t) := \hat{U}(t)\sigma_i^{\phi_{\rm s}}\hat{U}(t)^\dagger = \cos\phi_{\rm s}\sigma_i^x - \sin\phi_{\rm s}\hat{U}(t)\sigma_i^y \hat{U}(t)^\dagger$,

which can be expressed in terms of the m-th order Bessel functions $\mathfrak{J}_m(x)$ of the first class as follows

$$\sigma_i^{\phi_{\rm s}}(t) = \cos\phi_{\rm s}\sigma_i^x - \sin\phi_{\rm s}\sum_{m\in\mathbb{Z}} \mathfrak{J}_m\left(\xi\frac{h_0}{\Delta}\right)\cos\big((2h_0 + m\Delta)t\big)\sigma_i^y$$
$$+ \sin\phi_{\rm s}\sum_{m\in\mathbb{Z}} \mathfrak{J}_m\left(\xi\frac{h_0}{\Delta}\right)\sin\big((2h_0 + m\Delta)t\big)\sigma_i^z. \quad (A6)$$

Let us remark that the effect of the carrier driving (A3) on the full light-matter interaction of the MS scheme is to introduce a comb of new frequencies $\nu_{\pm,m} := \pm(2h_0 + m\Delta)$, where $m \in \mathbb{Z}$ (see Fig. 3(b)). Hence, the validity of the description of such a light-matter coupling in terms of the periodically-modulated MS force (A5) rests on the condition that none of these frequencies hits a resonance with the carrier or any higher-order sideband in the original light-matter interaction, or that in the event of such a resonance, the coupling strength gets suppressed in comparison with the aforementioned MS force. This imposes the following constraints on the carrier driving parameters

$$h_0 \sim \Delta \ll \omega_{n,x} \sim \omega_x, \quad \xi < \tfrac{1}{2}. \quad (A7)$$

The first inequality guarantees that the resonance will only occur for a very large number of 'photons' $m \gg 1$ absorbed from the drive (see Fig. 3(b)), whereas the second inequality guarantees that the strength of such a resonance gets exponentially suppressed with respect to the strength of the MS force as m increases (see Fig. 3(c)).

Provided that these conditions are met, we now start from Eq. (A5) to prove that the time-evolution operator in this transformed basis $\hat{U}(t) = \mathscr{T}\{{\rm e}^{-{\rm i}\int_0^t {\rm d}\tau \hat{H}_{\rm MS}(\tau)}\}$ gives raise to the desired effective XYZ Hamiltonian $\hat{U}(t) \approx {\rm e}^{-{\rm i}H_{\rm XYZ}t}$ in Eq. (2). We use the so-called Magnus expansion[31] to second order

$$\hat{U}(t) \approx {\rm e}^{\Omega_1(t) + \Omega_2(t)}, \quad \Omega_1(t) = -{\rm i}\int_0^t {\rm d}\tau \hat{H}_{\rm MS}(\tau), \quad \Omega_2(t) = -\frac{1}{2}\int_0^t {\rm d}\tau_1 \int_0^{\tau_1} {\rm d}\tau_2 [\hat{H}_{\rm MS}(\tau_1), \hat{H}_{\rm MS}(\tau_2)]. \quad (A8)$$

Integrating by parts, we find the following expression for the first-order contribution

$$\Omega_1(t) = \sum_{i,n} \frac{\mathscr{F}_{in} x_0}{\delta_n} a_n \left(\sigma_i^{\phi_{\rm s}}(t){\rm e}^{{\rm i}(\phi_{\rm m} - \delta_n t)} - \sigma_i^{\phi_{\rm s}}(0){\rm e}^{{\rm i}\phi_{\rm m}}\right) - \int_0^t {\rm d}\tau \frac{\mathscr{F}_{in} x_0}{\delta_n} \frac{{\rm d}\sigma_i^{\phi_{\rm s}}}{{\rm d}\tau} a_n {\rm e}^{{\rm i}(\phi_{\rm m} - \delta_n \tau)} - {\rm H.c.}, \quad (A9)$$

where the integral in the right hand side involves the derivative of the driven Pauli operator (A6). This first-order contribution to the unitary evolution can be understood as a spin-

dependent displacement acting on the phonons, and leading to spin-phonon correlations that compromise the validity of an effective spin model. As such, these terms must be minimised,
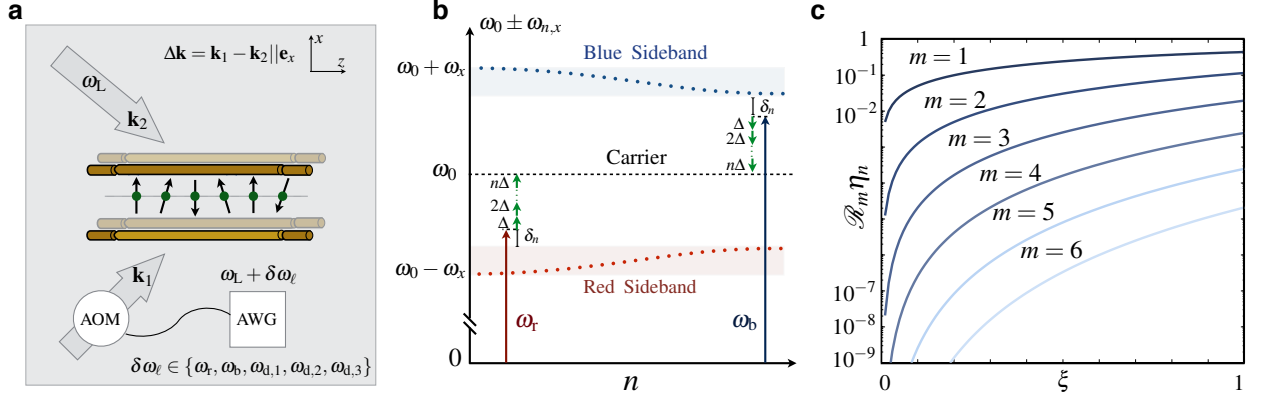
Figure 3. **Scheme of the quasi-periodically modulated Molmer-Sorensen force:** **(a)** Ions (green circles) forming a chain within the electrodes of a linear Paul trap. Two internal electronic levels of each ion form a pseudospin (thin arrows) that is coupled to the incident laser beams (wide arrows), the beatnote of which is controlled by an acusto-optical modulator (AOM) through an arbitrary wave generator (AWG). By using the different modulation frequencies in the AWG listed in Table I, we obtain a quasi-periodically modulated Molmer-Sorensen force that couples the spins to the motion along the axis $\mathbf{e}_x||\Delta\mathbf{k}$. **(b)** Scheme for the blue and red sidebands ($\omega_0 \pm \omega_{n,x}$) of the whole vibrational branch for the Molmer-Sorensen beams, and their symmetric detuning δ_n. We also represent with small arrows the comb of frequencies $m\Delta$, with $m \in \mathbb{Z}$, due to the additional drivings introduced in the scheme (A6), which could hit an undesired resonance (e.g. carrier transition). **(c)** Ratio of the coupling strength $\mathscr{R}_m$ between the possible spurious resonance with the carrier due to the additional comb of frequencies $m\Delta$, and the desired MS sideband, as a function of $m \in \{1, \cdots, 6\}$. We see that for the high resonances (i.e. high m) required by the constraint (A7), lead to a vanishingly small ratio, such that these terms can be safely neglected for the timescales of interest of the experiment.

which requires avoiding the possible new resonances brought up by the frequency comb of the driven Pauli operator (A6). This can be guaranteed by imposing a more restrictive constraint than Eq. (A7) on the carrier parameters

$$h_0 \sim \Delta \ll \delta_n \ll \omega_x, \quad \xi < \tfrac{1}{2}. \tag{A10}$$

Then, the integral in the right hand side is suppressed with respect to the left hand side, and

$$\Omega_1(t) \approx \sum_{i,n} \frac{\mathscr{F}_{in}x_0}{\delta_n} a_n \left(\sigma_i^{\phi_s}(t)e^{i(\phi_m-\delta_n t)} - \sigma_i^{\phi_s}(0)e^{i\phi_m} \right) - \text{H.c.},$$
(A11)

where we have neglected terms of the order $\mathscr{O}\left(\frac{\mathscr{F}_{in}x_0}{\delta_n}\frac{h}{\delta_n}\right)$. In order to make $\Omega_1(t) \approx 0$, we must thus work in the far-detuned regime of the MS force

$$\mathscr{F}_{in}x_0\sqrt{1+\bar{n}_n} \ll \delta_n, \tag{A12}$$

where $\bar{n}_n$ stands for the mean number of phonons of the ion chain after laser cooling has been performed. Hence, provided that the constraints in Eqs. (A10) and (A12) are fulfilled, the dynamics of the spins will be governed by the second-order contribution in Eq. (A8). This contribution can introduce terms that do not oscillate periodically in time and would thus not be negligible under the constraint (A12), but instead lead to an effective Hamiltonian. Once again, the integration by parts is of practical importance to identify the leading-order terms in the regime of Eq. (A10), and we find

$$\Omega_2(t) \approx -i\int_0^t d\tau \left(\sum_{i>j} J_{ij}\sigma_i^{\phi_s}(\tau)\sigma_j^{\phi_s}(\tau) + \sum_{i,n} \lambda_{in}\sigma_i^x(2a_{n,x}^\dagger a_{n,x}+1) \right),$$
(A13)

where we have neglected $\mathscr{O}\left(J_{ij}\frac{h}{\delta_n}\right)$ terms, and introduced the spin-spin couplings J_{ij} defined below Eq. (6) of the main text,

$$J_{ij} = -\sum_n \frac{\mathscr{F}_{in}\mathscr{F}_{jn}^*x_0^2}{\delta_n} + \text{c.c.}, \tag{A14}$$

and some residual spin-phonon coupling strength

$$\lambda_{in} = \sin^2\phi_s(\mathscr{F}_{in}x_0)^2 \sum_{m\in\mathbb{Z}} \mathfrak{J}_m^2\left(\frac{h_0}{\Delta}\xi\right) \frac{m\Delta+2h_0}{\delta_n^2-(m\Delta+2h)^2}. \tag{A15}$$

Since we have constrained the driving parameters to the regime in Eq. (A10), and we have in particular that $h_0 \sim \Delta$ and $\xi < \tfrac{1}{2}$, the m-photon resonances on the previous equation are exponentially suppressed as m increases, and we can approximate $\lambda_{in} = \sin^2\phi_s(\mathscr{F}_{in}x_0)^2\mathfrak{J}_0^2\left(\frac{h_0}{\Delta}\xi\right)2h_0/\delta_n^2 \sim \mathscr{O}\left(J_{ii}(1+2\bar{n}_n)\sin^2\phi_s \cdot h_0/\delta_n\right)$. According to this discussion, and provided that $h_0 \ll \delta_n$ (A10), this residual spin-phonon coupling becomes negligible, and we obtain an effective spin model described by a periodically-modulated Ising Hamiltonian

$$\tilde{U}(t) \approx \mathscr{T}\{e^{-i\int_0^t d\tau H_{\text{eff}}(\tau)}\}, \quad H_{\text{eff}}(\tau) = \sum_{i>j} J_{ij}\sigma_i^{\phi_s}(\tau)\sigma_j^{\phi_s}(\tau). \tag{A16}$$

In the numerical simulations presented in the main text, we explore what particular values of h_0, Δ, and ξ, fulfilling the above constraints, lead to a negligible spin-phonon coupling while simultaneously allowing for a wide tunability of the spin model.

The remaining task is to demonstrate that such a periodically-modulated Hamiltonian leads to the desired XYZ

model. So far, the derivation has only imposed that the strength and frequency of the carrier driving (A3) must have the same order of magnitude $h_0 \sim \Delta$. We will now show that by imposing a particular ratio h_0/Δ, it is possible to engineer the aforementioned XYZ model. Instead of using Eq. (A6), it will prove simpler to introduce the states

$|\pm_i\rangle = (|\uparrow_i\rangle \pm |\downarrow_i\rangle)/\sqrt{2}$, such that

$$\sigma_i^{\phi_s}(t) = \cos\phi_s\sigma_i^x - \sin\phi_s\left(\mathrm{i}e^{\mathrm{i}2h_0\left(t+\frac{\xi}{\Delta}\sin(\Delta t)\right)}|+_i\rangle\langle-_i| + \mathrm{H.c.}\right).$$
(A17)

We now substitute in the periodically-modulated spin model, and obtain $H_{\mathrm{eff}}(t) = \sum_{i>j}(h_{ij}^{(1)} + h_{ij}^{(2)} + h_{ij}^{(3)})$, where

$$
\begin{aligned}
h_{ij}^{(1)} &:= J_{ij}\cos^2\phi_s\sigma_i^x\sigma_j^x, \\
h_{ij}^{(2)} &:= J_{ij}\cos\phi_s\sin\phi_s\left(\sigma_i^x\left(\mathrm{i}e^{\mathrm{i}2h_0\left(t+\frac{\xi}{\Delta}\sin(\Delta t)\right)}|+_j\rangle\langle-_j| + \mathrm{H.c.}\right) + \left(\mathrm{i}e^{\mathrm{i}2h_0\left(t+\frac{\xi}{\Delta}\sin(\Delta t)\right)}|+_i\rangle\langle-_i| + \mathrm{H.c.}\right)\sigma_j^x\right), \\
h_{ij}^{(3)} &:= J_{ij}\sin^2\phi_s\left(\mathrm{i}e^{\mathrm{i}2h_0\left(t+\frac{\xi}{\Delta}\sin(\Delta t)\right)}|+_i\rangle\langle-_i| + \mathrm{H.c.}\right)\left(\mathrm{i}e^{\mathrm{i}2h_0\left(t+\frac{\xi}{\Delta}\sin(\Delta t)\right)}|+_j\rangle\langle-_j| + \mathrm{H.c.}\right).
\end{aligned}
$$
(A18)

In the contribution of $h_{ij}^{(2)}$, we obtain again the frequency comb in terms of multiples of the driving frequency, which contribute with terms that oscillate in time as follows $\sum_{m\in\mathbb{Z}} J_{ij}\mathfrak{J}_m\left(2\xi\frac{h_0}{\Delta}\right)e^{\mathrm{i}(2h_0+m\Delta)t}$. If we impose

$$\max\{J_{ij}\} \ll 2h_0 = \frac{\Delta}{2}$$
(A19)

all these terms can be neglected using a rotating wave approximation, such that $h_{ij}^{(2)} \approx 0$. The situation for $h_{ij}^{(3)}$ is different, as this term can be rewritten as follows

$$h_{ij}^{(3)} = J_{ij}\sin^2\phi_s\left(|+_i\rangle\langle-_i|\cdot|-_j\rangle\langle+_j| - \sum_{m\in\mathbb{Z}}\mathfrak{J}_m\left(4\xi\frac{h_0}{\Delta}\right)e^{\mathrm{i}(4h_0+m\Delta)t}|+_i\rangle\langle-_i|\cdot|+_j\rangle\langle-_j| + \mathrm{H.c.}\right).$$
(A20)

One thus finds that, under the constraints (A19), several terms can be neglected under a rotating-wave approximation, ex-

cept for certain of resonances that may be considered as a spin analogue of the photon-assisted tunnelling resonances in periodically-modulated quantum systems[32]. We thus obtain

$$h_{ij}^{(3)} \approx J_{ij}\sin^2\phi_s\left(|+_i\rangle\langle-_i|\cdot|-_j\rangle\langle+_j| - \mathfrak{J}_{-1}(\xi)|+_i\rangle\langle-_i|\cdot|+_j\rangle\langle-_j| + \mathrm{H.c.}\right).$$
(A21)

Remarkably enough, we get an effective time-independent Hamiltonian that can be rewritten as follows

$$H_{\mathrm{eff}}(t) \approx H_{\mathrm{XYZ}} = \sum_{i>j}\left(J_{ij}^x\sigma_i^x\sigma_j^x + J_{ij}^y\sigma_i^y\sigma_j^y + J_{ij}^z\sigma_i^z\sigma_j^z\right),$$
(A22)

where the different coupling constants have been written in Eq. (8) of the main text. If we consider the additional unitaries that were used to transform to the actual basis, we have shown that the full time-evolution of the driven trapped-ion crystal can be expressed as $U(t) \approx e^{-\mathrm{i}tH_0}e^{-\mathrm{i}\sum_i h_0\left(t+\frac{\xi}{\Delta}\sin(\Delta t)\right)\sigma_i^x}e^{-\mathrm{i}tH_{\mathrm{XYZ}}} =: U_0(t)e^{-\mathrm{i}tH_{\mathrm{eff}}}$, as used in the main text of this article.

Appendix B: Non-linear sigma model for a long-range Heisenberg Hamiltonian

In this Appendix, we present a detailed derivation of the mapping between the long-range anti-ferromagnetic Heisenberg model (LRHM), and the O(3) non-linear sigma model (NLSM). The LRHM is a lattice model of interacting spins obtained from Eqs. (2) and (8) after setting $\phi_s = \phi_s^c = \cos^{-1}(1/\sqrt{3})$ and $\xi = 0$, and described by the SU(2)-invariant spin Hamiltonian

$$H_{\mathrm{LRHM}} = \sum_{i>j}\tilde{J}_{ij}\boldsymbol{S}_i\cdot\boldsymbol{S}_j, \qquad \boldsymbol{S}_i = \frac{1}{2}(\sigma_i^x, \sigma_i^y, \sigma_i^z),$$
(B1)

where we have introduced $\tilde{J}_{ij} = 4J_{ij} > 0$. The NLSM is a relativistic quantum field theory in a 1+1 space-time $x^\mu = (vt, x)$ for a vector field $\boldsymbol{\phi}(x^\mu)$ on a 2-sphere, described by the Lagrangian density

$$\mathscr{L}_{\text{NLSM}} = \frac{1}{2g}(\partial_\mu \boldsymbol{\phi}) \cdot (\partial^\mu \boldsymbol{\phi}) + \frac{\Theta}{8\pi} \varepsilon^{\mu\nu} \boldsymbol{\phi} \cdot (\partial_\mu \boldsymbol{\phi} \times \partial_\nu \boldsymbol{\phi}), \quad \text{(B2)}$$

where $|\boldsymbol{\phi}(x^\mu)|^2 = 1$. Here, $g > 0$ is the coupling constant, $\varepsilon^{\mu\nu}$ is the Levi-Civita symbol, Θ is the so-called topological angle, and repeated indices are summed. By performing a Wick rotation $vt \to -i\tau$, the action associated to this Lagrangian is finite if $\lim_{|\boldsymbol{x}| \to \infty} \boldsymbol{\phi}(\boldsymbol{x}) = \boldsymbol{\phi}_0$. Hence, all values of the fields at infinity are the same $\boldsymbol{\phi}_0$, and the Euclidean space-time becomes isomorphic to a 2-sphere[57]. In this case, $\boldsymbol{\phi}(\boldsymbol{x})$ can be considered as a mapping of the 2-sphere of the compactified space-time onto the 2-sphere of the vector fields, and the Euclidean action can be written as $S = \int \mathrm{d}^2 x \mathscr{L}_{\text{NLSM}} = -\int \mathrm{d}^2 x \left(\frac{1}{2g}(\partial_\mu \boldsymbol{\phi})^2 + i\Theta W \right)$, where $W = \frac{1}{8\pi} \int \mathrm{d}^2 x \varepsilon^{\mu\nu} \boldsymbol{\phi} \cdot (\partial_\mu \boldsymbol{\phi} \times \partial_\nu \boldsymbol{\phi}) \in \mathbb{Z}$ is the winding number of the mapping. Since the action will be exponentiated in a path-integral approach, and $W \in \mathbb{Z}$, one directly sees that Θ is defined modulo 2π, and can be thus interpreted as an angle: a topological angle that controls the appearance of such a topological term in the action, and leads to important non-perturbative effects. For models invariant under parity $x^1 \to -x^1$, the invariance of the action imposes that $\Theta \in \{0, \pi\}$, which is responsible for the massive/massless character of the low-energy excitations of the NLSM, respectively.

In the nearest-neighbor limit of the LRHM (B1), Haldane showed that a mapping between both models exists and becomes exact in the large-S limit, where the spin-1/2 operators (B1) are substituted by spin-S operators that also fulfil the $\mathfrak{su}(2)$ algebra $[S_i^a, S_j^b] = i\varepsilon^{abc} S_i^c \delta_{i,j}$, but have magnitude $\boldsymbol{S}_i^2 = S(S+1)$[44]. The mapping leads to $g = 2/S$, $v = 2\tilde{J}Sa$, and $\Theta = 2\pi S \bmod(2\pi)$, where a is the lattice spacing. Accordingly, the topological angle vanishes $\Theta = 0$ for *integer spin*, and one recovers the standard NLSM without a topological term, which displays massive excitations, as shown by perturbative renormalization-group arguments for weak couplings $g \ll 1$[57,58], and series expansions for strong couplings $g \gg 1$[59]. This behaviour translates into exponentially-decaying spin-spin correlations and an energy gap in the spectrum, regardless of the value of the g, and thus valid for all different integer-S spin chains[44]. Conversely, one finds a NLSM with a topological term for *half-integer spin*, since $\Theta = \pi$, which modifies drastically the above properties. Building on the renormalisation-group flow to strong couplings, and thus small effective spins (as follows from $S = 2/g$), Haldane conjectured that all half-integer-spin Heisenberg models should be qualitatively identical to the $S = 1/2$ case, and should thus display algebraically-decaying correlations and a vanishing energy gap[36]. There is compelling evidence based on different numerical methods supporting such conjecture[60].

We now explore the effects of the long-range interactions on the mapping of the LRHM onto the NLSM. Let us start by reviewing the Hamiltonian approach to the NLSM described in[45,61], which starts by imposing directly the constraint over the vector field by introducing two scalar fields

$\alpha(x^\mu), \beta(x^\mu)$, such that $\boldsymbol{\phi} = (\sin\alpha\cos\beta, \sin\alpha\sin\beta, \cos\alpha)$. After obtaining their canonically-conjugate momenta through $\Pi_\alpha = \partial_{\dot\alpha} \mathscr{L}$, and $\Pi_\beta = \partial_{\dot\beta} \mathscr{L}$, one finds $\mathscr{H}_{\text{NLSM}} = \frac{1}{2g} \sum_\mu \left((\partial_\mu \alpha)^2 + \sin^2\alpha (\partial_\mu \beta)^2 \right)$ by using standard trigonometry. It is customary to introduce the angular momentum $\boldsymbol{\ell} = \boldsymbol{\phi} \times (\partial_\alpha \boldsymbol{\phi} \Pi_\alpha + \sin^{-2}\alpha \partial_\beta \boldsymbol{\phi} \Pi_\beta)$, and apply again basic trigonometric rules to obtain the final form of the NLSM Hamiltonian

$$H_{\text{NLSM}} = \int \mathrm{d}x \frac{v}{2} \left[g \left(\boldsymbol{\ell} - \frac{\Theta}{4\pi} \partial_x \boldsymbol{\phi} \right)^2 + \frac{1}{g}(\partial_x \boldsymbol{\phi})^2 \right], \quad \text{(B3)}$$

where $\boldsymbol{\phi}^2 = 1$, and $\boldsymbol{\ell} \cdot \boldsymbol{\phi} = 0$. Moreover, the following algebra between the vector and angular momentum fields is obtained

$$\begin{aligned}
[\phi^a(x), \phi^b(y)] &= 0, \\
[\ell^a(x), \phi^b(y)] &= i\varepsilon^{abc} \phi^c(x) \delta(x - y), \\
[\ell^a(x), \ell^b(y)] &= i\varepsilon^{abc} \ell^c(x) \delta(x - y),
\end{aligned} \quad \text{(B4)}$$

which follows from the canonical commutation relations of the scalar fields and their conjugate momenta.

The goal now is to find a particular NLSM Hamiltonian (B3) starting from the microscopic LRHM (B1), and introducing the following spin operators

$$\boldsymbol{\ell}_i = \frac{1}{2a}(\boldsymbol{S}_{2i+1} + \boldsymbol{S}_{2i}), \quad \boldsymbol{\phi}_i = \frac{1}{2S}(\boldsymbol{S}_{2i+1} - \boldsymbol{S}_{2i}), \quad \text{(B5)}$$

which represent small and rapid fluctuations of the local spin density, and slow fluctuations of the staggered spin density, respectively. Using the $\mathfrak{su}(2)$ spin algebra algebra, one finds that these operators satisfy the constraints

$$\boldsymbol{\ell}_i \cdot \boldsymbol{\phi}_i = 0, \quad \boldsymbol{\phi}_i^2 = 1 + \frac{1}{S} - \frac{\ell_i^2}{S^2}, \quad \text{(B6)}$$

which coincide with those of Eq. (B3) in the large-S and continuum $a \to 0$ limits. Moreover, the correct algebra is also recovered in these limits, since

$$\begin{aligned}
[\phi_i^a, \phi_j^b] &= i\varepsilon^{abc} \frac{\ell_i^c}{S^2} \frac{\delta_{i,j}}{2a}, \\
[\ell_i^a, \phi_j^b] &= i\varepsilon^{abc} \phi_i^c \frac{\delta_{i,j}}{2a}, \\
[\ell_i^a, \ell_j^b] &= i\varepsilon^{abc} \ell_i^c \frac{\delta_{i,j}}{2a},
\end{aligned} \quad \text{(B7)}$$

lead to Eqs. (B4) in the above limits, where $\frac{\delta_{i,j}}{2a} \to \delta(x - y)$. It is then clear that the local and staggered magnetisation (B5) shall play a key role in the mapping of the LRHM onto the NLSM.

Let us rewrite the LRHM (B1) as $H_{\text{LRHM}} = \sum_i \sum_r \tilde{J}_r \boldsymbol{S}_i \cdot \boldsymbol{S}_{i+r}$, which assumes that the spin-spin couplings are translationally invariant, and will thus describe the physics of the bulk of a large trapped-ion chain where such an approximation becomes valid (see the section below). Using the spin operators (B5), and partitioning the sum into even- and odd-spaced spin pairs, we find

$$H_{\text{LRHM}} = \sum_{i,r} \tilde{J}_{2r+1} \left(a^2 \boldsymbol{\ell}_i \cdot \boldsymbol{\ell}_{i+r} \quad + Sa(\boldsymbol{\ell}_i \cdot \boldsymbol{\phi}_{i+r} \quad - \boldsymbol{\phi}_i \cdot \boldsymbol{\ell}_{i+r} \quad) - S^2 \boldsymbol{\phi}_i \cdot \boldsymbol{\phi}_{i+r} \quad \right)$$
$$+ \sum_{i,r} \tilde{J}_{2r+1} \left(a^2 \boldsymbol{\ell}_i \cdot \boldsymbol{\ell}_{i+r+1} - Sa(\boldsymbol{\ell}_i \cdot \boldsymbol{\phi}_{i+r+1} - \boldsymbol{\phi}_i \cdot \boldsymbol{\ell}_{i+r+1}) - S^2 \boldsymbol{\phi}_i \cdot \boldsymbol{\phi}_{i+r+1} \right)$$
$$+ \sum_{i,r} \tilde{J}_{2r+2} \left(a^2 \boldsymbol{\ell}_i \cdot \boldsymbol{\ell}_{i+r+1} - Sa(\boldsymbol{\ell}_i \cdot \boldsymbol{\phi}_{i+r+1} + \boldsymbol{\phi}_i \cdot \boldsymbol{\ell}_{i+r+1}) + S^2 \boldsymbol{\phi}_i \cdot \boldsymbol{\phi}_{i+r+1} \right) \tag{B8}$$
$$+ \sum_{i,r} \tilde{J}_{2r+2} \left(a^2 \boldsymbol{\ell}_i \cdot \boldsymbol{\ell}_{i+r+1} + Sa(\boldsymbol{\ell}_i \cdot \boldsymbol{\phi}_{i+r+1} + \boldsymbol{\phi}_i \cdot \boldsymbol{\ell}_{i+r+1}) + S^2 \boldsymbol{\phi}_i \cdot \boldsymbol{\phi}_{i+r+1} \right).$$

The next step is to take the continuum limit, and make a gradient expansion keeping terms that are $\mathcal{O}(a^2)$. Then, it suffices to consider the following approximations for different pairs of integers $\{n, m\}$, namely

$$\boldsymbol{\ell}_n \cdot \boldsymbol{\ell}_{n+m} \to \boldsymbol{\ell}(x) \cdot \boldsymbol{\ell}(x+(2a)m) \approx \boldsymbol{\ell}^2(x),$$
$$\boldsymbol{\phi}_n \cdot \boldsymbol{\phi}_{n+m} \to \boldsymbol{\phi}(x) \cdot \boldsymbol{\phi}(x+(2a)m) \approx \boldsymbol{\phi}^2(x) + (2a)m\boldsymbol{\phi}(x) \cdot \partial_x \boldsymbol{\phi}(x) + \tfrac{1}{2}(2a)^2 m^2 \boldsymbol{\phi}(x) \cdot \partial_x^2 \boldsymbol{\phi}(x) \approx \left(1 + \tfrac{1}{S} - \tfrac{\boldsymbol{\ell}^2(x)}{S^2}\right) - 2a^2 m^2 (\partial_x \boldsymbol{\phi})^2,$$
$$\boldsymbol{\phi}_n \cdot \boldsymbol{\ell}_{n+m} \to \boldsymbol{\phi}(x) \cdot \boldsymbol{\ell}(x+(2a)m) \approx \boldsymbol{\phi}(x) \cdot \boldsymbol{\ell}(x) + (2a)m\boldsymbol{\phi}(x) \cdot \partial_x \boldsymbol{\ell}(x) = -(2a)m\boldsymbol{\ell}(x) \cdot \partial_x \boldsymbol{\phi}(x),$$
$$\boldsymbol{\ell}_n \cdot \boldsymbol{\phi}_{n+m} \to \boldsymbol{\ell}(x) \cdot \boldsymbol{\phi}(x+(2a)m) \approx \boldsymbol{\ell}(x) \cdot \boldsymbol{\phi}(x) + (2a)m\boldsymbol{\ell}(x) \cdot \partial_x \boldsymbol{\phi}(x) = (2a)m\boldsymbol{\ell}(x) \cdot \partial_x \boldsymbol{\phi}(x). \tag{B9}$$

To arrive at these expressions, we have performed the corresponding Taylor expansions for $a \to 0$, used the lattice constraints (B6), and considered integration by parts under $\sum_i (2a) \to \int dx$ assuming that the fields vanish at the boundaries of the sample. Under these approximations, the Hamiltonian of the LRHM becomes

$$H_{\text{LRHM}} \approx \int dx \left[2a \sum_r \tilde{J}_{2r+1} \boldsymbol{\ell}^2(x) - Sa \sum_r \tilde{J}_{2r+1} \left(\boldsymbol{\ell}(x) \cdot \partial_x \boldsymbol{\phi}(x) + \partial_x \boldsymbol{\phi}(x) \cdot \boldsymbol{\ell}(x) \right) - \frac{Sa^2}{2} \sum_r (-1)^r r^2 J_r (\partial_x \boldsymbol{\phi}(x))^2 \right]. \tag{B10}$$

By direct comparison with the Hamiltonian (B3) of the NLSM, we find a system of three algebraic equations that leads to the following NLSM parameters

$$v = 2aS \sqrt{\sum_{r \text{ odd}} \tilde{J}_r \left(\sum_{r \text{ odd}} r^2 \tilde{J}_r - \sum_{r \text{ even}} r^2 \tilde{J}_r \right)},$$
$$g = \frac{2}{S} \sqrt{\sum_{r \text{ odd}} \tilde{J}_r \left(\sum_{r \text{ odd}} r^2 \tilde{J}_r - \sum_{r \text{ even}} r^2 \tilde{J}_r \right)^{-1}}, \tag{B11}$$
$$\Theta = 2\pi S.$$

As a consistency check, we note that in the nearest-neighbor limit $\tilde{J}_r = \tilde{J}\delta_{r,1}$ with $\tilde{J} > 0$, we recover the same parameters for

the mapping of the Heisenberg model onto the NLSM, namely $v = 2\tilde{J}aS, g = 2/S$, and $\Theta = 2\pi S$, which lead to Haldane's conjecture.

In the main text, we evaluate the above coupling constant g for the particular spin-spin couplings that arise in the trapped-ion scenario. It is also very interesting to consider long-range interactions that decay with a power-law of the distance

$$\tilde{J}_r = \frac{\tilde{J}_1}{r^s}, \tag{B12}$$

with an exponent $s > 0$. In the thermodynamic limit, the series appearing in Eq.(B11) can be expressed in terms of Dirichlet η and λ functions, that in turn are related in a simple way to the Riemann zeta function ζ,

$$\sum_{r \text{ odd}} \tilde{J}_n = \sum_{n=0}^{\infty} \frac{\tilde{J}_1}{(2n+1)^s} = \tilde{J}_1 \lambda(s) = \tilde{J}_1 (1 - 2^{-s}) \zeta(s), \quad \text{Re}\, s > 1 \tag{B13}$$

$$\sum_{r \text{ odd}} r^2 \tilde{J}_r - \sum_{r \text{ even}} r^2 \tilde{J}_r = \sum_{n=1}^{\infty} \frac{\tilde{J}_1 (-1)^{1+n}}{n^{s-2}} = \tilde{J}_1 \eta(s-2) = \tilde{J}_1 (1 - 2^{3-s}) \zeta(s-2), \quad \text{Re}\, s > 2 \tag{B14}$$

The convergence of these two series requires that $s > 2$. In the limit $s \to 2$, the series Eq.(B14) is Abel convergent, which

means that it can be regularized by adding a term e^{-xn}, with $x > 0$, and then taking the limit $x \to 0$. This gives the well known result $1 - 1 + 1 + \cdots = 1/2$. In this case one obtains the the Haldane-Shastry model where the exchange couplings decreases as in inverse square distance[46]. The values of v and g are given by

$$s = 2 \implies v = 4\pi a J_1, \qquad g = 2\pi. \tag{B15}$$

Appendix C: Distance decay of the effective spin-spin interactions

In this Appendix, we derive explicit formulas for the distance dependence of the phonon-mediated spin-spin interactions in the trapped-ion crystal (A14). If we consider the small Lamb-Dicke parameter, which is particularly the case for heavy ions such as ^{171}Yb$^+$, and also take into account additional off-resonant terms in the MS scheme[12], the spin-spin interactions can be written as

$$J_{ij} = \frac{|\Omega_{\mathrm{L}}|^2}{2} \omega_{\mathrm{R}} \sum_n \frac{\mathscr{M}_{i,n} \mathscr{M}_{j,n}^*}{\mu^2 - \omega_{n,x}^2} + \mathrm{c.c.}, \tag{C1}$$

where we have introduced the recoil energy $\omega_{\mathrm{R}} = (\Delta \mathbf{k} \cdot \mathbf{e}_x)^2 / 2m$, and the symmetric beatnote of the MS beams $\omega_{\mathrm{b}} = \omega_0 + \mu, \omega_{\mathrm{r}} = \omega_0 - \mu$, which corresponds to $\mu = \omega_{n,x} - \delta_n$ according to our previous notation. It is straightforward to see that in the resolved-sideband limit considered throughout this work $|\delta_n| \ll \omega_n$, one can approximate $\mu^2 - \omega_{n,x}^2 = (\mu + \omega_{n,x})(\mu - \omega_{n,x}) \approx -2\omega_{n,x}\delta_n$. Hence, by using the expression of the MS forces (A1) for small Lamb-Dicke parameters $\eta_n \ll 1$, we see that Eq. (C1) is equivalent to the spin-spin couplings derived in Eq. (A14). Nonetheless, it will be useful to use the full expression (C1) instead of (A14) in the derivation of the distance decay of the spin-spin couplings. Let us emphasise that, although a power-law decay with a tunable exponent $s \in [0,3]$, namely $J_{ij} = \tilde{J}_0/|i-j|^s$, serves as a convenient approximation in experiments[26,28,43,62], special care must be taken when such expressions are to be extrapolated to the thermodynamic limit in theoretical studies. This is particularly so for the evaluation of the NLSM parameters (B11), which crucially depend on the long-range tail of the spin-spin couplings.

In Ref.[63], it was shown that if Eq. (A14) is approximated further by considering $\mu^2 - \omega_{n,x}^2 \approx -2\omega_{n,x}\delta_n \approx -2\omega_x\delta_n$, it is possible to derive an analytical estimate of the spin-spin couplings by using a continuum limit, and substituting the sum over the normal modes by an integral that can be evaluated by an extension to the complex plane. Provided that $\mu < \omega_{n,x}$, it was shown that J_{ij} has two contributions: a term that displays a dipolar decay, and another one that shows an exponential tail with a characteristic decay length dominated by the detuning of the spin-dependent force with respect to the lowest-energy zig-zag mode. It is by varying this characteristic length that

the spin-spin couplings show a variable range that can be seen as an effective power law $J_{ij} = \tilde{J}_0/|i-j|^\alpha$ that is slower than the dipolar decay $\alpha < 3$ for sufficiently small chains. However, let us remark again that for theoretical extrapolations to very large ion chains, one should use directly the correct distance dependence.

We will now show that a similar result can be obtained without making the approximation $\mu^2 - \omega_{n,x}^2 \approx -2\omega_x\delta_n$ in Eq. (C1), and independently of the choice of $\mu \lessgtr \omega_{n,x}$, as far as the force is far from the resonance with any mode in the vibrational band $\mu \neq \omega_{n,x}$. We shall not resort to a continuum limit, but partially resume the most relevant terms of Eq. (C1). Since we are interested in the predictions of the mapping of the spin chain onto the NLSM (B11), which are only valid for the bulk of the trapped-ion crystal, we use a homogeneous lattice spacing a_0 that corresponds to the distance between two neighbouring ions in the centre of the chain. Following[63], we describe the normal-mode displacements and frequencies of the ion crystal by

$$\mathscr{M}_{j,n} = \frac{1}{\sqrt{N}} e^{iqa_0 j}, \qquad \omega_{n,x} = \sqrt{\tilde{\omega}_x^2 + 2\beta_x \omega_x^2 \sum_{d=1}^{N/2} \frac{c_d}{d^3} \cos(qa_0 d)}, \tag{C2}$$

where we have used periodic boundary conditions, such that it is possible to introduce the quasi-momentum within the Brillouin zone $q = 2\pi n/Na_0 \in \mathrm{BZ} = [0, 2\pi/a_0)$, the coefficients $c_d = (1 - \delta_{d,N/2}) + \delta_{d,N/2}/2$, and a renormalised trap frequency $\tilde{\omega}_x = \omega_x (1 - 2\beta_x \sum_d c_d/d^3)^{1/2}$ that depends on the stiffness parameter $\beta_x = (e^2/4\pi\varepsilon_0 a_0)/m\omega_x^2 a_0^2$[10]. We now substitute Eq. (C2) in the expression (C1), and use the geometric Taylor series for $|\lambda| < 1$, in order to express the spin-spin couplings as follows

$$J_{i,j} = \frac{J_0}{N} \sum_{q \in \mathrm{BZ}} \sum_{n=0}^{\infty} e^{iqa_0(i-j)} \lambda^n \left(\sum_{d=1}^{N/2} \frac{c_d}{d^3} \cos(qa_0 d) \right)^n + \mathrm{c.c.}, \tag{C3}$$

where we have introduced two important parameters in our calculations

$$J_0 = \frac{|\Omega_{\mathrm{L}}|^2 \omega_{\mathrm{R}}}{2(\mu^2 - \tilde{\omega}_x^2)}, \qquad \lambda = \frac{2\beta_x \omega_x^2}{(\mu^2 - \tilde{\omega}_x^2)}. \tag{C4}$$

If $\mu^2 > \tilde{\omega}_x^2 + 2\beta_x \omega_x^2$, the beatnote of the MS laser beams will be off-resonant with respect to the whole vibrational branch. Therefore, assuming that $|\lambda| < 1$ requires working at sufficiently-large MS detunings $|\delta_n| > \beta_x \omega_x$, a fact that is in any case required to minimise the error of the quantum simulator for a spin chain[10].

To proceed further, we approximate $\left(\sum_d \frac{c_d}{d^3} \cos(qa_0 d) \right)^n \approx \cos^n(qa_0) + n \sum_{d>1} \frac{c_d}{d^3} \cos(qa_0 d)$, which is justified given the fast dipolar decay of these couplings. By finally making use of the binomial theorem, we find that $J_{ij} = J_{ij}^{(1)} + J_{ij}^{(2)}$, where
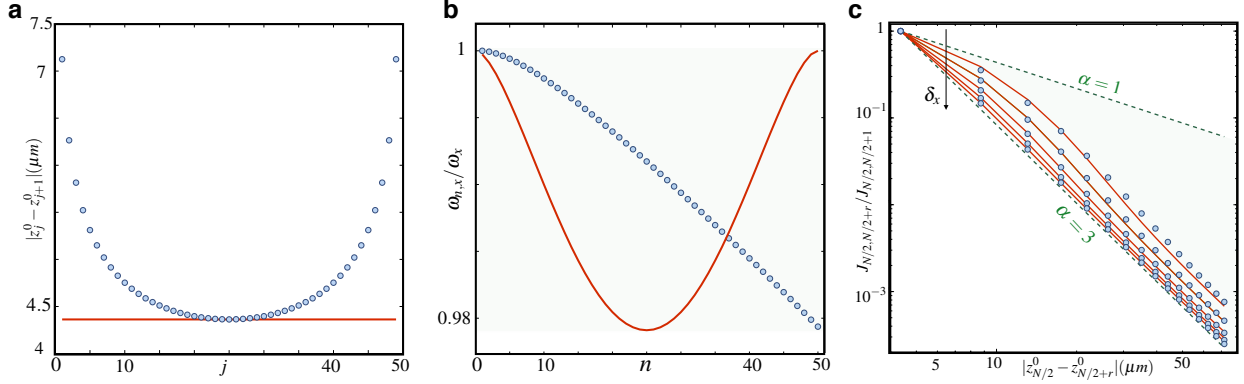
Figure 4. **Distance dependence of the spin-spin couplings:** (a) Distance between neighbouring ions $|z_j^0 - z_{j+1}^0|$ as a function of the lattice index $j \in \{1, \cdots, 49\}$ for a chain of $N = 50$ Yb ions. The blue circles are obtained from the exact equilibrium positions $z_j^0 = \ell_z u_j$ by solving $u_j - \sum_{k \neq j}(u_j - u_k)/|u_j - u_k|^3 = 0$, where $\ell_z = (e^2/4\pi\varepsilon_0 m\omega_z^2)^{1/3}$. The red line stands for the theoretical model of a homogeneous ion chain $z_j^0 = a_0 j$ with constant lattice spacing given by $a_0 = \min\{|z_j^0 - z_{j+1}^0|\}$. (b) Normalized vibrational frequencies $\omega_{n,x}/\omega_x$ as a function of the normal-mode index $n \in \{1, \cdots, 50\}$. The blue circles represent the exact normal modes obtained by solving $\sum_{ij} \mathcal{M}_{i,n} \mathbb{K}_{i,j} \mathcal{M}_{j,m} = \omega_{n,x}^2 \delta_{n,m}$, where $\mathbb{K}_{i,j}/\omega_x^2 = (1 - \delta_{i,j})\beta_x/|z_i^0 - z_j^0|^3 + \delta_{i,j}(1 - \sum_{l \neq i} \beta_x/|z_i^0 - z_l^0|^3)$ is obtained from the numerical solution of the equilibrium positions in the inhomogeneous crystal. The red line stands for the theoretical model for a homogeneous periodic chain with the normal modes given in Eq. (C2). (c) Normalised spin-spin couplings $J_{i,j}/J_{i,i+1}$ between the central ion $i = N/2 = 25$ and its bulk neighbours $j = N/2 + r$, with $r \in \{1, \cdots 16\}$, as a function of their respective distance $|z_i^0 - z_j^0|$, and for different values of the MS detuning $\delta_x = \omega_x - \mu$ with respect to the center-of-mass mode, $\delta_x/2\pi \in \{62.5, 125, 250, 500, 1000\}$kHz, increasing in the direction of the arrow. The blue circles are obtained by solving Eq. (C1) using the previous normal modes and frequencies. The red lines stand for our analytical result (C6) without any fitting parameter, but rather using the microscopic values for Eqs. (C4) and (C8). The green dashed lines correspond to a power-law decay $J_r \propto 1/r^s$ for two different exponents $s = 3$, and $s = 1$.

$$J_{ij}^{(1)} = \frac{J_0}{N} \sum_{q \in \text{BZ}} \sum_{n=0}^{\infty} \sum_{k=0}^{n} \left(\frac{\lambda}{2}\right)^n \binom{n}{k} e^{iqa_0\left((i-j)+n-2k\right)} + \text{c.c.},$$

$$J_{ij}^{(2)} = \frac{J_0}{N} \sum_{q \in \text{BZ}} \sum_{n=0}^{\infty} \sum_{k=0}^{n-1} \sum_{d=2}^{N/2} \frac{c_d}{d^3} n \left(\frac{\lambda}{2}\right)^n \binom{n-1}{k} \left(e^{iqa_0\left((i-j)+n-1-2k+d\right)} + e^{iqa_0\left((i-j)+n-1-2k-d\right)} \right) + \text{c.c.}. \tag{C5}$$

To evaluate these expressions, we need to make use of the sum of angles in the complex unit circle $\sum_{q \in \text{BZ}} e^{iqa_0 x} = N\delta_{x,0}$, and a number of combinatorial identities. By introducing $r = i - j$ and $J_{ij} = J_{i-j} =: J_r$, we find $J_r = J_r^{(1)} + J_r^{(2)}$ with

$$J_r^{(1)} = 2|J_0|(\text{sgn}(\lambda))^{1+|r|} e^{-\frac{|r|a_0}{\xi_0}}, \tag{C6}$$

and

$$J_r^{(2)} = \sum_{\delta r = 2-r}^{N/2-r} |J_0\lambda| (\text{sgn}(\lambda))^{1+|\delta r|} \frac{c_{r+\delta r}}{|r+\delta r|^3} \left(\frac{\sqrt{1-\lambda^2} + |\delta r|(1-\lambda^2)}{(1-\lambda^2)^2} \right) e^{-\frac{|\delta r|a_0}{\xi_0}} \theta(r-2), \tag{C7}$$

where we have introduced the following decay length associated to the exponential terms

$$\xi_0 = -\frac{a_0}{\log\left(\frac{1-\sqrt{1-\lambda^2}}{|\lambda|}\right)}, \tag{C8}$$

and the Heaviside step function, $\theta(x) = 1$ if $x \geq 0$ and zero elsewhere.

Let us now comment on the different possible regimes. In the limit of $\lambda \to 0$, the exponential terms decay very rapidly since $\xi_0 \to 0$, and we find $J_r^{(1)} \approx |J_0\lambda|\delta_{r,1}$, $J_r^{(2)} \approx |J_0\lambda|/|r|^3 \theta(r-2)$. Therefore, for very large detunings of the MS force such that $\lambda \to 0$, we recover the well-known antiferromagnetic dipolar limit of the phonon-mediated spin-spin interactions $J_r \approx \tilde{J}_0/|r|^3$, where $\tilde{J}_0 =$

$|J_0\lambda| = |\Omega_L|^2\omega_R\beta_x\omega_x/8\omega_x\delta_x^2 > 0$[10]. On the other hand, for finite but still small $|\lambda| \ll 1$, we find that the leading order corrections to the dipolar tail come from an exponentially-decaying term

$$J_r \approx \frac{|J_0\lambda|}{|r|^3} + 2|J_0|\left(\text{sgn}(\lambda)\right)^{1+|r|}e^{-\frac{|r|a_0}{\xi_0}}\theta(r-2), \qquad (C9)$$

a result similar to that found in[63], but valid for red/blue detunings without making any further approximation to Eq. (C1). The detuning of the MS forces can be understood as an effective mass m_{eff} of the phonons that carry the spin-spin interactions. This effective mass would naturally account for an exponential decay of the interactions with length $\xi \propto 1/m_{\text{eff}}$, which would be combined with the natural dipolar decay associated to a system for transversally-oscillating charges (i.e. effective dipoles). As $|\lambda|$ grows larger $0 < |\lambda| < 1$, the complete expression in Eq. (C6) must be considered, as the different exponentials can lead to considerable modifications of the spin-spin couplings.

We should now test the validity of our result (C6) by comparing with a numerically-exact evaluation of the spin-spin couplings (C1) using the equilibrium positions and normal modes[22] for a ion crystal with the realistic parameters introduced in the main text. We consider $N = 50$ ^{171}Yb$^+$ ions in a linear Paul trap with frequencies $\omega_z/2\pi = 0.1$MHz, and $\omega_x/2\pi = 5$MHz, which form an inhomogeneous chain with minimal lattice spacing $a_0 = 4.4\mu$m corresponding to two neighbouring ions in the centre of the chain (see Fig. 4(a)). In this figure, we see that the lattice spacing of the finite ion chain is inhomogeneous, and varies considerably when approaching the chain boundaries. We also display the theoretical model of a constant lattice spacing to describe the bulk of the ion crystal. The vibrational frequencies $\omega_{n,x}$ are displayed in Fig. 4(b), where we compare the exact numerical values with those obtained by using a periodic ion chain with homogeneous lattice spacing (C2). We observe that the vibrational bands have the same width in both cases, while the doubling of the vibrational frequencies is a consequence of the periodic boundary conditions as opposed to the open boundary conditions of a realistic chain. Despite the clear differences in Figs. 4(a) and 4(b), we shall now show that the theoretical model gives very accurate results for the spin-spin interactions of bulk ions in the inhomogeneous ion chain. In Fig. 4(c), we compare the exact spin-spin couplings for the inhomogeneous ion chain (C1), with the analytical estimates (C6) based on the theoretical model of the periodic homogeneous ion chain (C2). The agreement between both values is quite remarkable, given the relatively small size of the ion chain, and the clear differences displayed in Figs. 4(a) and 4(b). Let us highlight that the considered detunings in the MS forces correspond to $\lambda \in [0.04, 0.4]$, and thus to some instances where the parameter λ is far from being a small perturbation.

We can also identify the qualitative behaviour described below Eq. (C6): for very large MS detunings, the distance-dependence can be reliably approximated by a dipolar law. As the detunings decrease, and thus the relevant parameter λ increases, the contribution of an exponential tail to the spin-spin couplings starts playing a role. This becomes apparent for the couplings J_r at small distances $ra_0 \ll \xi_0$, where we see a decay that is much slower than the dipolar law. However, at large distances $ra_0 \gg \xi_0$, the contribution from the exponential tail is suppressed, and one recovers the dipolar power law. These numerical results confirm that the analytical estimates (C6) are more accurate than a fit to a power-law decay $J_r \propto 1/r^s$ with a varying exponent $s \in [0,3]$. Let us finally remark that, in order to obtain an analytical expression for even larger interaction ranges, one should take into account further terms in the approximation above Eq. (C5), which may become relevant for sufficiently-small detunings. In any case, such small MS detunings compromise the validity of a pure effective spin model, as errors due to a thermal phonon population start playing a dangerous role[10].

[1] R. P. Feynman, Int. J. Theor. Phys. **21,** 467 (1982).

[2] J. I. Cirac and P. Zoller, Nat. Phys. **8,** 264 (2012).

[3] *See* I. Bloch, J. Dalibard, and S. Nascimbène, Nat. Phys. **8,** 267 (2012), *and references therein.*

[4] *See* R. Blatt and C. F. Roos, Nat. Phys. **8,** 277 (2012), *and references therein.*

[5] S. Lloyd, Science **23,** 1073 (1996).

[6] J. H. Shirley, Phys. Rev. **138,** B979 (1965).

[7] *See*, A. Eckardt, arXiv:1606.08041 (2016), *and references therein.*

[8] *See*, A. Verdeny, J. Puig, and F. Mintert, arXiv:1603.03923 (2016), *and references therein.*

[9] D. J. Wineland, C. Monroe, W. M. Itano, D. Leibfried, B. E. King, and D. M. Meekhof, J. Res. Natl. I. St. Tech. **103,** 259 (1998).

[10] D. Porras and J. I. Cirac, Phys. Rev. Lett. **92,** 207901 (2004); X.-L. Deng, D. Porras, and J. I. Cirac, Phys. Rev. A **72,** 063407 (2005).

[11] A. Friedenauer, H. Schmitz, J. T. Glueckert, D. Porras, and T. Schaetz, Nat. Phys. **4,** 757 (2008); K. Kim, M.-S. Chang, S. Korenblit, R. Islam, E. E. Edwards, J. K. Freericks, G.-D. Lin, L.-M. Duan, and C. Monroe, Nature **465,** 590 (2010); R. Islam, E. E. Edwards, K. Kim, S. Korenblit, C. Noh, H. Carmichael, G.-D. Lin, L.-M. Duan, C.-C. Joseph Wang, J.K. Freericks, and C. Monroe, Nat. Comm. **2,** 377 (2011).

[12] C. Monroe, W. C. Campbell, E. E. Edwards, R. Islam, D. Kafri, S. Korenblit, A. Lee, P. Richerme, C. Senko, and J. Smith, *Proceedings of the International School of Physics Enrico Fermi*, Course 189, pp. 169-187, edited by M. Knoop, I. Marzoli, and G. Morigi (2015).

[13] P. Pfeuty, Ann. Phys. **57,** 79 (1970).

[14] S. Sachdev, *Quantum Phase Transitions* (Cambridge University Press, Cambridge, 1999).

[15] H.-J. Mikeska, and A. K. Kolezhuk, *One-dimensional Magnetism*, Lect. Notes Phys. **645,** 1-83 (2004).

[16] W. Heisenberg, Z. Phys. **49,** 619 (1928).

[17] H. A. Bethe, Z. Phys. **71,** 205 (1931).

[18] B. P. Lanyon, C. Hempel, D. Nigg, M. Müller, R. Gerritsma, F. Zähringer, P. Schindler, J. T. Barreiro, M. Rambach, G. Kirch-

mair, M. Hennrich, P. Zoller, R. Blatt, and C. F. Roos, Science **334,** 57 (2011).

[19] I. Arrazola, J. S. Pedernales, L. Lamata, and E. Solano, Sci. Rep. **6,** 30534 (2016).

[20] R. J. Baxter, Phys. Rev. Lett. **26,** 834 (1971); R. J. Baxter, Ann. Phys. **70,** 323 (1972).

[21] C. N. Yang and C. P. Yang, Phys. Rev. **150,** 321 (1966); (ibid.) **150,** 327 (1966); (ibid.) **151,** 258 (1966).

[22] D.F.V. James, Appl. Phys. B **66,** 181 (1998).

[23] A. Sorensen and K. Molmer, Phys. Rev. Lett. **82,** 1971 (1999); A. Sorensen, and K. Molmer, Phys. Rev. A **62,** 022311 (2000) ; C. A. Sackett, D. Kielpinski, B. E. King, C. Langer, V. Meyer, C. J. Myatt, M. Rowe, Q. A. Turchette, W. M. Itano, D. J. Wineland, and C. Monroe, Nature **404,** 256 (2000); J. Benhelm, G. Kirchmair, C. F. Roos, R. Blatt, Nat. Phys. **4,** 463 (2008).

[24] P. J. Lee, K.-A. Brickman, L. Deslauriers, P. C. Haljan, L.-M. Duan, and C. Monroe, J. Opt. B: Quantum Semiclass. Opt. **7,** S371 (2005).

[25] T. Schaetz, A. Friedenauer, H. Schmitz, L. Petersen, and S. Kahra, J. Mod. Opt. **54,** 2317 (2007); R. Schmied, J. H. Wesenberg, D. Leibfried, Phys. Rev. Lett. **102,** 233002 (2009); A. C. Wilson, Y. Colombe, K. R. Brown, E. Knill, D. Leibfried, and D. J. Wineland, Nature **512,** 57 (2014); M. Mielenz, H. Kalis, M. Wittemer, F. Hakelberg, R. Schmied, M. Blain, P. Maunz, D. Leibfried, U. Warring, and T. Schaetz, Nat. Commun. **7,** 11839 (2016).

[26] J. W. Britton, B. C. Sawyer, A. C. Keith, C.-C. J. Wang, J. K. Freericks, H. Uys, M. J. Biercuk, and J. J. Bollinger, Nature **484,** 489 (2012); J. G. Bohnet, B. C. Sawyer, J. W. Britton, M. L. Wall, A. M. Rey, M. Foss-Feig, J. J. Bollinger, Science **352,** 1297 (2016).

[27] A. Bermudez, P. O. Schmidt, M. B. Plenio, and A. Retzker, Phys. Rev. A **85,** 040302(R) (2012); A. Lemmer, A. Bermudez, M. B. Plenio, New J. Phys. **15,** 083001 (2013); T. R. Tan, J. P Gaebler, R. Bowler, Y. Lin, J. D. Jost, D. Leibfried, and D. J. Wineland, Phys. Rev. Lett. **110,** 263002 (2013).

[28] P. Richerme, Z.-X. Gong, A. Lee, C. Senko, J. Smith, M. Foss-Feig, S. Michalakis, A. V. Gorshkov, and C. Monroe, Nature **511,** 198 (2014); P. Jurcevic, B. P. Lanyon, P. Hauke, C. Hempel, P. Zoller, R. Blatt, C. F. Roos, Nature **511,** 202 (2014).

[29] T. Graß, M. Lewenstein, and A. Bermudez, New J. Phys. **18,** 033011 (2016).

[30] S. Fernandez-Lorenzo, J. J. Garcia-Ripoll, and D. Porras, New J. Phys. **18,** 023030 (2016).

[31] W. Magnus, Commun. Pure Appl. Math. **7,** 649 (1954); S. Blanes, F. Casas, J. A. Oteo and J. Ros, Eur. J. Phys. **31,** 907 (2010).

[32] D. H. Dunlap and V. M. Kenkre, Phys. Rev. B **34,** 3625 (1986).

[33] S. Olmschenk, K. C. Younge, D. L. Moehring, D. N. Matsukevich, P. Maunz, and C. Monroe, Phys. Rev. A **76,** 052314 (2007).

[34] M. A. Nielsen, Phys. Lett. A **303,** 249 (2002).

[35] For $\xi = 0$, Eq. (2) coincides with the famous XXZ Heisenberg model[15] in a rotated spin basis.

[36] A. Luther and I. Peschel, Phys. Rev. B **12,** 3908 (1975); F. D. M. Haldane, Phys. Rev. Lett. **45,** 1358 (1980).

[37] F. D. M. Haldane, Phys. Rev. B **25,** 4925(R) (1982); K. Okamoto, and K. Nomura, Phys. Lett. A **169,** 433 (1992).

[38] A. A. Nersesyan, A. O. Gogolin, and F. H. L. Eler, Phys. Rev. Lett. **81,** 910 (1998); T. Hikihara, M. Kaburagi, and H. Kawamura, Phys. Rev. B **63,** 174430 (2001).

[39] For $N/2$ odd, we require a staggered version of the transverse field $\sum_i h\sigma_i^y \rightarrow \sum_i h(-1)^i\sigma_i^y$. Experimentally, it may be easier to substitute $\sigma_j^y \rightarrow \sigma_j^z$, which could be implemented through local

[40] ac-Stark shifts in the trapped-ion experiment, and would require an initial state $|\psi_0\rangle = |\downarrow\uparrow\downarrow\cdots\rangle$.

For N odd, the groundstate can display additional degeneracies, as can be easily seen from the Jordan-Wigner fermion solution of the nearest-neighbor XY model $\phi_s = \pi/2$[41], when applied to open boundary conditions. We avoid these by considering only N even.

[41] E. H. Lieb, T. Schultz, and D. J. Mattis, Ann. Phys. **16,** 407 (1961).

[42] W. H. Zurek, U. Dorner, and P. Zoller, Phys. Rev. Lett. **95,** 105701 (2005).

[43] C. Senko, J. Smith, P. Richerme, A. Lee, W. C. Campbell, C. Monroe, Science **345,** 430 (2014); P. Jurcevic, P. Hauke, C. Maier, C. Hempel, B. P. Lanyon, R. Blatt, and C. F. Roos, Phys. Rev. Lett. **115,** 100501 (2015).

[44] F. D. M. Haldane, Phys. Lett. A **93,** 464 (1983); F. D. M. Haldane, Phys. Rev. Lett. **50,** 1153 (1983).

[45] I. Affleck, *Les Houches Proceedings*, in Fields, strings and critical phenomena, eds. E Brezin and J. Zinn-Justin, (North-Holland, Amsterdam, 1988).

[46] F. D. Haldane, Phys. Rev. Lett. **60,** 635 (1988); B. S. Shastry, Phys. Rev. Lett. **60,** 639 (1988).

[47] J. I. Cirac and G. Sierra, Phys. Rev. B **81,** 104431 (2010).

[48] G. Sierra, *El Escorial Proceedings*, in Lectures Notes in Physics **478,** eds. G. Sierra and M.A. Martin-Delgado, (Springer-Verlag, Berlin, 1997).

[49] I. Cohen and A. Retzker, Phys. Rev. Lett. **112,** 040503 (2014); C. Senko, P. Richerme, J. Smith, A. Lee, I. Cohen, A. Retzker, and C. Monroe, Phys. Rev. X **5,** 021026 (2015); I. Cohen, P. Richerme, Z.-X. Gong, C. Monroe, A. Retzker, Phys. Rev. A **92,** 012334 (2015).

[50] Z.-X. Gong, M. F. Maghrebi, A. Hu, M. L. Wall, M. Foss-Feig, and A. V. Gorshkov, Phys. Rev. B **93,** 041102 (2016); Z.-X. Gong, M. F. Maghrebi, A. Hu, M. Foss-Feig, P. Richerme, C. Monroe, and A. V. Gorshkov, Phys. Rev. B **93,** 205115 (2016).

[51] J. Haegeman, J. I. Cirac, T. J. Osborne, I. Pizorn, H. Verschelde and F. Verstraete, Phys. Rev. Lett. **107,** 070601 (2011).

[52] T. Koffel, M. Lewenstein and L. Tagliacozzo, Phys. Rev. Lett. **109,** 267203 (2012).

[53] P. Hauke and L. Tagliacozzo, Phys. Rev. Lett. **111,** 207202 (2013).

[54] *See* P. Calabrese, and J. Cardy, J. Phys. A: Math. Theor. **42,** 504005 (2009), *and references therein*.

[55] We have checked that our numerical routine yields the predicted central charge $c = 1$ for the nearest-neighbour limit of the Heisenberg model, using the same bond dimension $\chi = 256$ of the Matrix-Product-State.

[56] *See* I. Affleck, N. Laflorencie, and E. S. Sørensen, J. Phys. A: Math. Theor. **42,** 504009 (2009), *and references therein*.

[57] E. Fradkin, *Field Theories of Condensed Matter Physics* (Cambridge University Press, Cambridge, 2013).

[58] A. M. Polyakov, Phys. Lett. B **59,** 79 (1975).

[59] C. J. Hamer, John B. Kogut, and L. Susskind, Phys. Rev. D **19,** 3091 (1979).

[60] S.R. White, D.A. Huse, Phys. Rev. B **48,** 3844 (1993); O. Golinelli, Th. Jolicur, R. Lacaze, Phys. Rev. B **50,** 3037 (1994); S. Todo and K. Kato, Phys. Rev. Lett. **87,** 047203 (2001).

[61] I. Affleck, Nuc. Phys. B **257,** 397 (1985).

[62] R. Islam, C. Senko, W. C. Campbell, S. Korenblit, J. Smith, A. Lee, E. E. Edwards, C.-C. J. Wang, J. K. Freericks, and C. Monroe, Science **340,** 583 (2013).

[63] P. Nevado and D. Porras, Phys. Rev. A **93,** 013625 (2016).